ORIGIN, INJECTION, AND ACCELERATION OF CIR PARTICLES: OBSERVATIONS

Report of Working Group 6

G. M. MASON[1] AND R. VON STEIGER[2]
CO-CHAIRS

R. B. DECKER[3], M. I. DESAI[1], J. R. DWYER[1], L. A. FISK[4], G. GLOECKLER[1,4], J. T. GOSLING[5], M. HILCHENBACH[6], R. KALLENBACH[2], E. KEPPLER[6], B. KLECKER[7], H. KUNOW[8], G. MANN[9], I. G. RICHARDSON[1,10], T. R. SANDERSON[11], G. M. SIMNETT[12], Y.-M. WANG[13], AND R. F. WIMMER-SCHWEINGRUBER[14]
PARTICIPANTS

M. FRÄNZ[15] AND J. E. MAZUR[16]
CONTRIBUTING AUTHORS NOT PARTICIPATING IN THE WORKSHOP

[1]*Dept. of Astronomy and IPST, University of Maryland, College Park, Maryland, USA*
[2]*International Space Science Institute, Bern, Switzerland*
[3]*Applied Physics Laboratory, John Hopkins University, Laurel, Maryland, USA*
[4]*Dept. of Atmospheric and Space Sciences, University of Michigan, Ann Arbor, Michigan, USA*
[5]*Los Alamos National Laboratory, Los Alamos, New Mexico, USA*
[6]*Max-Planck-Institut für Aeronomie, Katlenburg-Lindau, Germany*
[7]*Max-Planck-Institut für Extraterrestrische Physik, Garching, Germany*
[8]*Extraterrestrische Physik, Universität Kiel, Kiel, Germany*
[9]*Astrophysikalisches Institut, Potsdam, Germany*
[10]*NASA Goddard Space Flight Center, Greenbelt, Maryland, USA*
[11]*Space Science Dept. of ESA/ESTEC, Noordwijk, The Netherlands*
[12]*Physics and Astronomy Dept., University of Birmingham, Birmingham, United Kingdom*
[13]*E.O. Hulburt Center for Space Research, Naval Research Laboratory, Washington, DC, USA*
[14]*Physikalisches Institut der Universität Bern, Bern, Switzerland*
[15]*Queen Mary and Westfield College, London, United Kingdom*
[16]*Aerospace Corporation, Los Angeles, California, USA*

Received: 4 November 1998; Accepted: 25 May 1999

Abstract. This report emphasizes new observational aspects of CIR ions revealed by advanced instruments launched on the Ulysses, WIND, SOHO, and ACE spacecraft, and by the unique vantage point of Ulysses which carried out the first survey of Corotating Interaction Region (CIR) properties over a very wide range of heliolatitudes. With this more complete observational picture established, this review is the basis to consider the status of theoretical models on origin, injection, and acceleration of CIR particles reported by Scholer, Mann *et al.* (1999) in this volume.

Space Science Reviews **89:** 327–367, 1999.

1. Introduction

G. M. MASON

Observations in the 1970s and 1980s established the basic observational features of CIR energetic particle populations, as summarized in the accompanying paper by Mason and Sanderson (1999), namely that the ions were energized by forward and reverse shocks with peak intensities at several AU where the shocks became fully formed. The general similarity of the CIR heavy ion abundances with solar system abundances made the solar wind a likely candidate for the seed populations, although puzzling overabundances of elements such as He and C indicated that this picture was not fully satisfactory. It became evident that CIR energetic particles may be used to investigate the seed population(s) of different ion species in the heliosphere. During this same period, much progress was made in understanding the nature of particle acceleration at interplanetary shocks, and a theory combining acceleration and transport was developed by Fisk and Lee (1980), which successfully predicted spectral forms at 1 AU. Unlike solar energetic particle events, CIRs may be observed *in situ* giving a coordinated picture of the full range of field, plasma, and energetic particle properties. In the last few years, new instruments have helped set a more complete foundation for these studies. Comprehensive measurements of the solar wind composition have been carried out for the first time, yielding the basic features of the widely-assumed seed population, and in particular identifying differences between high- and low-speed solar wind composition that is particularly relevant to CIR studies. In addition, pick-up ions have been identified first at 1 AU, and later as a function of radius out to 5 AU during the Ulysses mission. The pick-up ions, whose peak velocity at twice the solar wind speed may give them a crucial boost in efficiency for acceleration, are an important new element of the picture.

New particle instruments on Ulysses, WIND, SOHO, and ACE and the on-going studies on Voyager, have established features of the energy spectra, and temporal development of CIRs. For example, Ulysses spectral measurements at mid-latitudes have revealed spectral forms harder than would be expected from the local field and plasma measurements. Voyager observations of similar spectral forms over a huge range of heliocentric distances are another puzzle. At 1 AU, observation of CIR related power law spectra down to energies just merging with the solar wind show the presence of particles that would have great difficulty propagating inward from the presumed source at several AU. This picture is reinforced by the difference in pick-up He, which is only about 20% of the CIR He population at 1 AU, in contrast to the situation at 5 AU where the pick-up He is roughly 2/3 of the CIR He population. Another unexpected development has been the observation of a C/O ratio that is a strong function of solar wind speed – with variations far outside the expectation for solar wind values. Lastly, non-field aligned transport has been observed during the most intense periods of some large CIRs, which may have critical bearing for acceleration and transport issues. These new finding are summarized below.

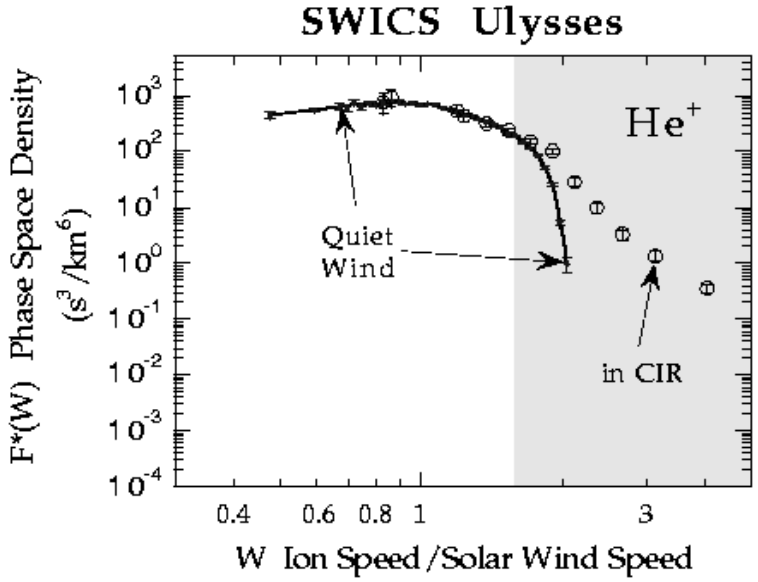

Figure 1. Phase-space density *vs. W* (ion speed/solar wind speed) of $^4He^+$ during a one-day period (starting 19 October 1991 0400 UT) behind the forward shock of a CIR normalized to the quiet time $^4He^+$ spectrum in the high speed solar wind (Gloeckler and Geiss, 1998) for *W* below ∼1.6. In the CIR the average solar wind He bulk speed was 387 km/s and Ulysses was in the ecliptic plane at 4.49 AU from the Sun. The CIR spectrum has a pronounced high-energy tail above *W* ∼1.8 showing clear evidence of acceleration of pickup He.

2. Seed Populations

G. GLOECKLER and J. T. GOSLING

The solar wind has long been considered the natural source for the energetic particle population observed in CIRs, as summarized, *e. g.*, by Fisk and Lee (1980). This source is reviewed elsewhere in this volume (Gloeckler, 1999). Below we review recent evidence for additional sources such as pickup ions, and consider as well the outstanding problem of electron acceleration in CIRs.

2.1. Accelerated Pick-up Ions in the Disturbed Solar Wind Inside a CIR

Pickup ion velocity distributions observed in the turbulent solar wind, such as the wind inside CIRs have a distinctly different character, showing unmistakable evidence for strong heating and acceleration. This is best illustrated for $^4He^+$, a pure pickup ion species. In Fig. 1 we compare the phase-space density versus *W* (the ion speed divided by the solar wind speed) of $^4He^+$ measured with the Solar Wind Ion Composition Spectrometer (SWICS) on Ulysses at 4.49 AU during a one day period immediately behind the forward shock of a CIR, to that found in the quiet high speed solar wind (Gloeckler and Geiss, 1998). The quiet wind distribution has

been scaled by 2.3 to account for the different loss and production rates during the two time periods. What is clearly observed is that while the quiet time spectrum has a sharp cutoff at $W=2$ indicating negligible energy diffusion and acceleration, the CIR spectrum has a pronounced high-velocity tail showing unmistakable acceleration above $W\sim1.6$. Below W of ~1.6 the two spectra are virtually identical. We conclude, in agreement with Gloeckler *et al.* (1994) and Schwadron *et al.* (1996), that in the turbulent solar wind (as is the case behind the CIR shocks) pickup $^4He^+$ ions are easily pre-accelerated. These pre-accelerated ions may then be readily injected for further acceleration to MeV energies by shocks. Thus, the once puzzling ubiquitous presence of energetic (0.4-0.6 MeV/amu) $^4He^+$ measured during a $\sim$1.5 year period in 1978/79 at 1 AU by Hovestadt *et al.* (1984), can now be quite naturally explained to be interstellar pickup $^4He^+$ accelerated in CIRs at $\sim$3 to 6 AU.

The proton velocity distribution in CIRs is more complex because of the presence of both solar wind and interstellar pickup protons of comparable densities in the critical range of W between 1.6 and 2. This is illustrated in the upper panel of Fig. 2 where we compare the phase-space density of protons (open circles) in the CIR (same time period as in Fig. 1) with the H^+ spectrum measured in the quiet high speed solar wind (Gloeckler and Geiss, 1998). Again the quiet wind distribution has been scaled to take account of the larger production rate of pickup protons in the CIR. In comparing the two spectra two differences stand out. First, the solar wind distribution around $W\sim1$ is much broader and very non-Maxwellian. The dotted curve is a kappa function fit with V_{th}=33 km/s and an extremely low value of κ=2.7, compared to 40 km/s and 12 for the quiet period. The high-velocity tail of this distribution, extrapolated to speed beyond $W=2$ still falls far below the observed distribution for $W>2$. In fact this high-velocity tail, resulting from protons accelerated in the CIR is the second obvious difference between the CIR and the quiet-time spectra. Assuming that the protons in the tail have been energized from those in the $\sim1.6<W<\sim2$ speed interval (as suggested by the $^4He^+$ observations discussed previously), which contains roughly comparable densities of solar wind and pickup protons, we conclude that the accelerated protons in the high-velocity tail are a mixture containing at least as many pickup protons as solar wind protons (see also Gloeckler *et al.*, 1994).

To further explore the question of what source material is injected into the acceleration mechanism producing energetic CIR particles we examine the velocity distribution of $^4He^{++}$ (lower panel of Fig. 2), which, in the critical W range of 1.6 to 2, has also both the heated solar wind α particles and pickup $^4He^{++}$ produced by double charge exchange from solar wind α particles (Gloeckler *et al.*, 1997). Indeed there is a discernible hump in the $^4He^{++}$ velocity distribution indicating the presence of pickup $^4He^{++}$. The spectra of $^4He^+$ and H^+ are normalized to that of $^4He^{++}$ above $W\sim2$ by dividing them by 7 and 100 respectively. We note that the tails of all three distributions have identical shapes (within experimental uncertainties) indicating a velocity dependent acceleration. Furthermore, there is

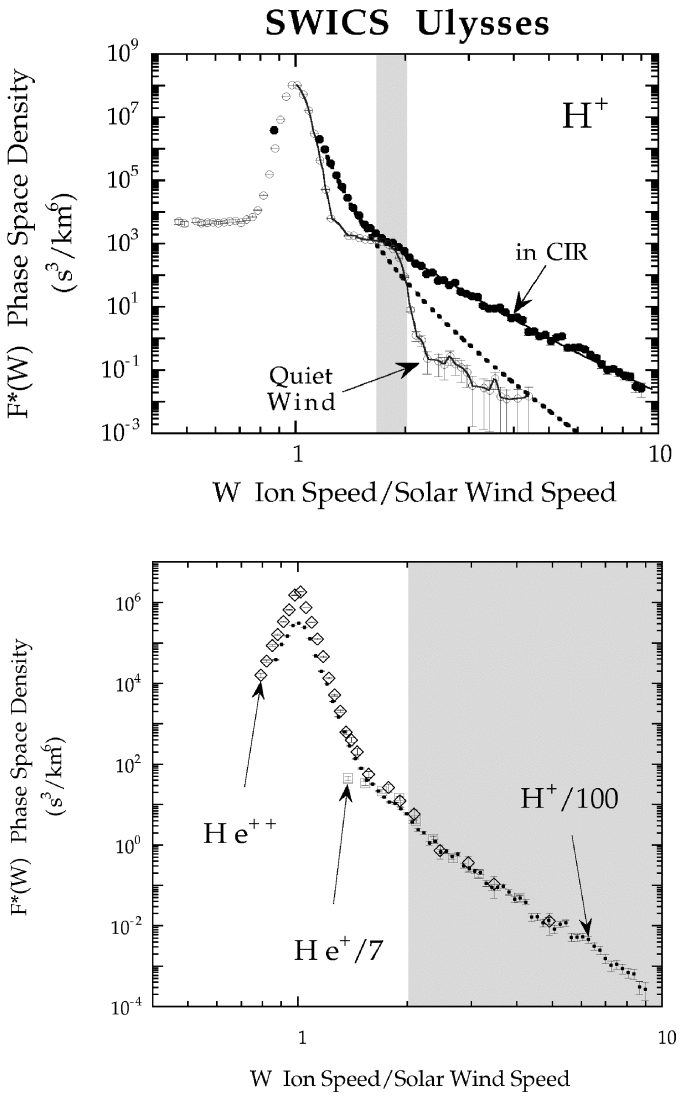

Figure 2. Upper panel: Same CIR event as Fig. 1 for H^+. The quiet time H^+ spectrum in the high speed solar wind (Gloeckler and Geiss, 1998) has been normalized to the CIR spectrum at $W \sim 1.8$. As was the case for the He^+ CIR spectrum, the H^+ CIR velocity distribution also has a pronounced high-energy tail above $W \sim 1.8$. Because of significant heating of solar wind protons the density in the critical W range of ~ 1.6 to 2 is comparable for these two ion populations. Thus it is likely that about equal proportions of pickup and solar wind ions have been accelerated in this region of the CIR. The dotted curve is a kappa function fit to the heated solar wind proton distribution extrapolated beyond W of ~ 1.6. In the solar wind frame the high speed proton tail has a power law dependence on speed with index -5 up to the highest observable speed. *Lower panel:* Superposition of the CIR H^+, He^+ and He^{++} velocity distributions. The H^+ and He^+ phase-space density was divided by 100 and 7 respectively to give equal densities in the high velocity tail above $W = 2$. We note that (a) the tails of all three ion species have the same shape, (b) the He^+/He^{++} ratio in the tail is ~ 7, and (c) the $H^+/(He^+ + He^{++})$ ratio is about 12.

at least seven times more pickup He than solar wind He in the tail, and probably more like a factor of ∼15 more because about half of the $^4He^{++}$ in the tail are pickup He. We can therefore conclude from this comparison that the He detected at MeV energies during this time interval is predominantly accelerated pickup He. The $^4He^{++}/H^+$ ratio in the tail is 0.01 compared to about 0.03 for the solar wind. If one assumes that the half of accelerated $^4He^{++}$ is solar wind $^4He^{++}$ (with the other half being accelerated pickup $^4He^{++}$), and that the same fraction of solar wind protons is accelerated into the tail, then the ratio of accelerated pickup hydrogen to solar wind protons is about 5. Even if we make the extreme assumption that the accelerated $^4He^{++}$ is all solar wind the ratio of accelerated pickup protons to solar wind protons is still 2, that is more pickup protons than solar wind protons are accelerated.

Just how much of the solar wind versus pickup ions are accelerated in CIRs will depend on the fraction of these populations in the critical W range above ∼1.6. Had the solar wind been heated slightly more (*e. g.* slightly smaller value of κ) than was the case here, then the composition in the tail (and hence also in the MeV range) would have been more solar wind like. On the other hand, had the bulk solar wind speed been higher than was the case here, then even a higher ratio of pickup to solar wind ions would have been accelerated.

2.2. Suprathermal Electrons Upstream of Forward and Reverse CIR Shocks

A field-aligned flux of suprathermal electrons with energies ranging from about 20 eV to greater than 200 eV is commonly observed upstream from both the forward and the reverse shocks that bound CIRs at heliocentric distances greater than ∼2 AU (Gosling *et al.*, 1993a). This flux consists of shock-heated and accelerated solar wind electrons that subsequently escape back upstream. These electrons counterstream relative to the hot suprathermal electrons (the halo population) that carry the solar wind electron heat flux away from the Sun; thus, they are directed sunward along the interplanetary magnetic field (IMF). Fluxes of these electrons are usually strongest immediately upstream of the shocks, and decrease gradually with increasing distance from them. On average, as observed by Ulysses, these counterstreaming fluxes persist for ∼58 hours upstream of the shocks, although durations vary considerably from one shock to another. An interesting aspect of these events is that the flux of suprathermal electrons streaming outward from the Sun commonly increases and decreases in concert with the flux of suprathermal electrons backstreaming from the shock. This appears to be a result of mirroring and scattering of the backstreaming beam sunward of the observation point.

Figure 3 helps summarize these observations in terms of the global magnetic field geometry thought to be associated with CIRs (Palmer and Gosling, 1978). Indeed, these events provide the strongest possible demonstration that the field geometry sketched in the figure is the pertinent one for CIRs. With increasing

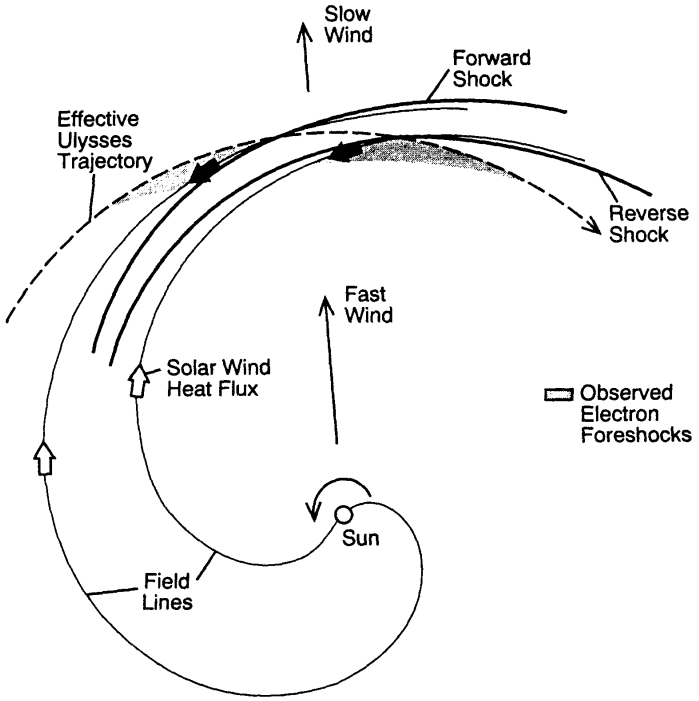

Figure 3. Schematic showing inferred IMF-CIR shock geometry. Shading indicates relative intensity and spatial extent of shock-associated suprathermal electrons events. Heavy arrows indicate the propagation direction of the shock-associated electrons (adapted from Gosling *et al.*, 1993a).

heliocentric distance the shocks bounding a CIR diverge from one another as the forward shock propagates into the slow plasma ahead while the reverse shock propagates backward into the high-speed plasma. Owing to solar rotation, the shocks are roughly aligned with Archimedean spirals when the flow is time stationary. At such times, field lines and stream lines in the solar wind flow coincide in a frame of reference corotating with the Sun, so that field lines intersect the shocks in the manner drawn in the figure. Thus the normals for both shocks face back to the Sun along the IMF. The entire pattern corotates with the Sun even though each parcel of plasma moves outward nearly radially. The dashed line in the figure shows the effective trajectory of Ulysses through the corotating pattern. Shading along the orbit indicates the regions (not to scale) where these counterstreaming fluxes are observed and the relative intensity of the fluxes (decreasing with distance from the shocks). All of the sunward-moving fluxes observed originate from beyond the position of the spacecraft. It can be shown that typical distances along the IMF from Ulysses to the shocks at the outermost edges of the "foreshocks" are of the order of 15 AU. Magnetic field connections to the shocks at greater distances typically do not produce measurable fluxes of backstreaming electrons at the spacecraft owing at least in part to the effects of scattering and mirroring in transit to the spacecraft.

The backstreaming electrons events described here provide an excellent means of determining when a spacecraft is magnetically connected to a CIR shock and, in conjunction with more energetic particle measurements, may provide a means of distinguishing between magnetic field models such as those of Fisk (1996) and Kóta and Jokipii (1983).

3. Plasma and Shock Parameters

G. MANN

The interaction of fast and slow solar wind streams leads to the formation of a pair of forward and reverse shock waves at the boundaries of the CIRs. The forward shocks propagate into the slow wind towards the equatorial plane of the heliosphere. The reverse shocks travel polewards into the fast solar wind stream. In this section these shocks will be considered from a magnetohydrodynamical point of view. Then, they can be characterized by few dimensionless parameters presented in Table I.

In general a shock wave is a dissipative structure at which kinetic energy of a streaming fluid is transferred into heat. Considering shock waves as plane travelling discontinuities in magnetohydrodynamics they can be described in terms of conservation of mass, momentum, energy, and magnetic flux without the knowledge of the special process of dissipation. This is conveniently done in the de Hoffmann-Teller frame, in which the shock is at rest and the motional electric field is removed in the upstream region (Priest, 1982). All downstream quantities can be determined by the upstream ones. For instance the density jump $n = N_2/N_1$ (N_2 particle number density in the down-stream region; N_1 particle number density in the upstream region) across the shock is found as a zero of the polynomial

$$\begin{aligned} 0 \;=\; & (m_A^2 - n)^2 \left\{\gamma\beta n + m_A^2 \cos^2(\theta_{Bn}) \left[(\gamma - 1)n + (\gamma + 1)\right]\right\} \\ & + m_A^2 n \sin^2(\theta_{Bn}) \left\{\left[\gamma + (2 - \gamma)n\right] m_A^2 - n\left[(\gamma + 1) - n(\gamma - 1)\right]\right\} \end{aligned} \tag{1}$$

The jump of the magnetic field $b = B_2/B_1$ (B_2 downstream magnetic field; B_1 upstream magnetic field) is related to the density jump n according to

$$b = \sqrt{\cos^2(\theta_{Bn}) + \frac{(m_A^2 - 1)^2}{(m_A^2 - n)^2} n^2 \sin^2(\theta_{Bn})} \tag{2}$$

Equations 1 and 2 represent the well-known jump or *Rankine-Hugoniot* relationships (Priest, 1982). Here, γ denotes the adiabatic index. Then, a shock can be characterized by few dimensionless parameters, *i. e.*, Alfvén-Mach number $M_A = v_i/v_{A1}$ as the ratio between the flow speed v_1 and the Alfvén velocity $v_{A1} = B_1/(4\pi m_p N_1)^{1/2}$ in the upstream region, the plasma beta, $\beta = 8\pi N_1 k_B T_1/B_1^2$, as the ratio between the thermal and magnetic pressure in the upstream region, and the angle θ_{Bn} between the upstream magnetic field and the shock normal (T_1, upstream temperature; m_p,

TABLE I
Parameters of CIR related shocks

No	year	day	B_1 (nT)	B_2/B_1	N_1 (cm^{-3})	N_2/N_1	θ_{Bn} (°)	β	M_A
1F	1992	185	0.70	1.70	0.25	1.40	54	0.35	1.60
1R	1992	188	0.65	1.73	0.16	1.70	77	0.52	1.90
2F	1992	202	0.75	2.17	0.33	2.30	59	0.31	2.20
2R	1992	205	0.55	1.90	0.15	3.10	20	0.34	2.70
$3F_1$	1992	226	1.20	1.21			67		
$3F_2$	1992	229	2.10	1.11	0.32	1.25	73	0.10	1.30
$3R_2$	1992	233	1.20	1.59	0.35	1.40	52	0.84	1.50
$3R_1$	1992	234	0.70	1.62	0.15	1.70	43	0.64	1.80
4F	1992	257	3.00	1.44	0.60	1.70	51	0.40	1.60
4R	1992	259	0.45	3.73	0.05	2.60	64	0.43	5.30
5F	1992	282	1.50	1.35	0.60	1.40	75	0.23	1.42
5R	1992	285	0.50	2.46	0.12	2.30	68	0.83	3.00
6F	1992	307	0.50	1.88	0.10	3.10	82	0.28	2.37
6R	1992	310	0.80	2.60	0.27	2.20		1.17	
7F	1992	334	0.51	1.83	0.09	3.30	42	0.82	2.97
7R	1992	336	0.40	3.00	0.05	3.00		0.54	
8F	1992	361	0.75	1.56	0.18	2.00	25	0.22	1.70
8R	1992	364	0.70	2.45	0.10	2.20	70	0.35	2.74
9F	1993	020	1.00	1.57	0.80	2.00	72	2.08	2.47
9R	1993	022	0.75	2.94	0.20	2.40	69	0.99	4.33
l0F	1993	051	0.55	1.14	0.07	1.90	28	0.18	1.20
l0R	1993	053	0.70	2.73	0.14	2.50	72	0.45	3.00
11F	1993	076	0.55	1.73	0.24	1.70	42	0.65	1.90
11R	1993	079	0.85	1.65	0.25	1.60	57	2.30	2.40
12R	1993	105	1.70	1.66	0.20	1.40	29	0.48	1.60
13R	1993	130	1.00	2.07	0.20	2.50	59	1.38	3.10
14R	1993	156	0.80	1.99	0.20	1.75	36	2.27	3.00
15F	1993	180	0.80	2.20	0.18	1.72	65	0.98	2.70
15R	1993	183	0.90	2.29	0.15	1.50	19	1.16	2.80
16R	1993	207	0.75	2.09	0.20	2.00	39	0.99	3.10
17R	1993	244	0.40	1.50			46		
18R	1993	261	0.90	1.77	0.90	1.50	65	1.15	2.10

TABLE II
Mean values of the shock parameters of forward and reverse shocks

mean values	B_2/B_1	N_2/N_1	$\theta_{Bn}(^\circ)$	β	M_A
forward shocks	1.62	2.0	57	0.55	2.0
reverse shocks	2.20	2.1	52	0.94	2.8

proton mass; k_B, Boltzmann's constant). M_A is related to m_A by $M_A = m_A \cos(\theta_{Bn})$ (*cf.* Eqs. 1 and 2).

Table I presents these dimensionless parameters of all CIR related shocks during the southbound passage of Ulysses. The data are adapted from the papers by Balogh *et al.* (1995) and Classen *et al.* (1998) based on the measurements of the SWOOPS solar wind plasma instrument (Bame *et al.*, 1992) and the magnetometer (Balogh *et al.*, 1992) aboard Ulysses. It should be noted that the CIRs 1, 4, 6, 11, and 15 were influenced by coronal mass ejections (CMEs) and/or travelling interplanetary shocks.

The mean values of the shock parameters are separately given for the 13 forward and 19 reverse shocks in Table II. The reverse shocks are mostly accompanied by a stronger jump of the magnetic field and a higher Alfvén-Mach number than the forward shocks.

As already mentioned, shock waves are dissipative structures. Resistivity alone cannot provide all the dissipation needed for satisfying the *Rankine-Hugoniot* relations (Marshall, 1955) if the Alfvén-Mach number M_A of the shock is greater than a critical one. The critical Alfvén-Mach number M_A^* is defined by equating the normal component of the downstream flow speed in the shock frame to the sound speed in the downstream region (Edmiston and Kennel, 1984). It depends on the plasma beta β and the angle θ_{Bn}. Under heliospheric circumstances between 1 and 5 AU M_A^* lies in the range 1.3–2.3. Classen *et al.* (1998) analyzed CIR related shocks with respect to this critical Alfvén-Mach number M_A^* and found that the forward and reverse shocks are predominantly sub-critical ($M_A < M_A^*$) and super-critical ($M_A > M_A^*$) respectively. In a collisionless plasma, shock waves with $M_A > M_A^*$ need some additional dissipation mechanism. A part of the incoming ions are nearly specularly reflected at super-critical shocks (Gosling *et al.*, 1982). For $\theta_{Bn} > 45^\circ$, the guiding center motion of these specularly reflected ions is directed downstream (Schwartz *et al.*, 1983). Thus, these ions are able to penetrate into the downstream region, where they contribute to ion thermalization (Sckopke *et al.*, 1983). For $\theta_{Bn} < 45^\circ$ the guiding center motion of the specularly reflected ions is directed upstream, if the upstream magnetic field is steady (Schwartz *et al.*, 1983). But these ions are able to excite plasma waves in the upstream region (Thomsen *et al.*, 1985). These plasma waves scatter a part of the reflected ions back towards the downstream region, where they can contribute to ion thermalization. This demonstrates the role of reflected ions for the shock dissipation (Gosling and Robson, 1985). Even super-critical shocks are able to accelerate particles up to

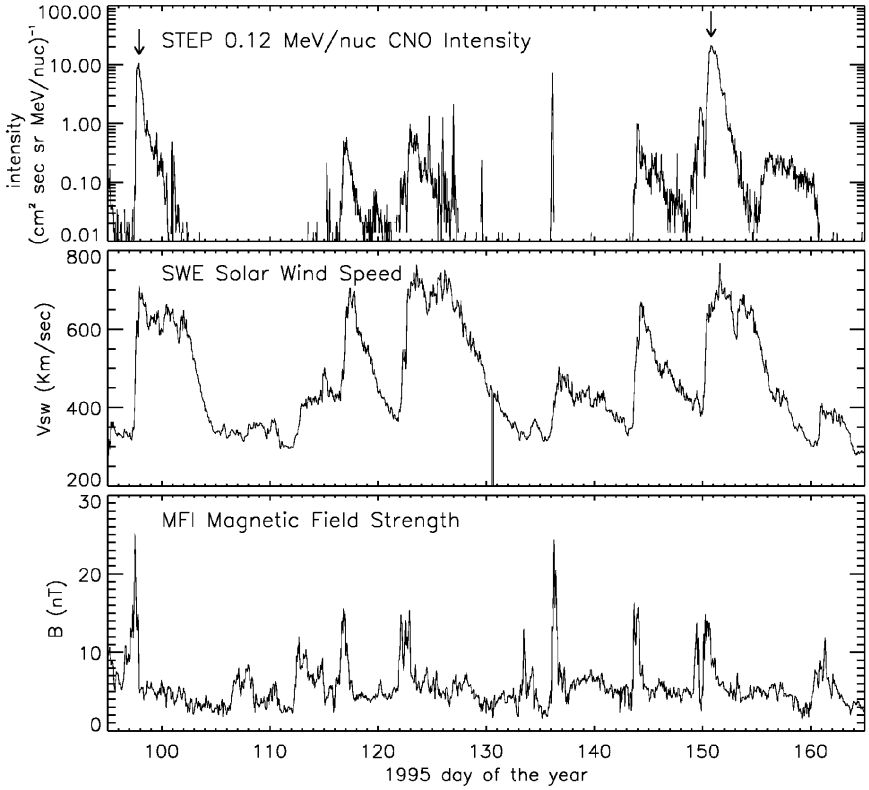

Figure 4. Top panel: 0.08–0.16 MeV/amu CNO intensity as measured by the STEP instrument for the time period containing the April 7, 1995, (day 97) and May 30, 1995, (day 150) CIRs (arrows). *Middle panel:* Solar wind speed as measured by SWE onboard Wind. *Bottom panel:* Magnetic field strength as measured by MFI onboard WIND. Note that the day 97 and day 150 CIRs correspond to the same high speed wind structure separated by two solar rotations.

high energies (Kennel *et al.*, 1985). The relationship between particle acceleration at CIR related shocks and their MHD parameters is discussed in Sect. 5.1.

4. Time-intensity Profiles and Spectral Evolution at 1 AU

J. R. DWYER, R. B. DECKER, and H. KUNOW

For the first two years after the November 1994 launch of the WIND spacecraft, the majority of intense particle enhancements observed at 1 AU, originating from outside the Earth's environment, were associated with CIRs, the most intense of these occurring at the end of 1994 and during the first six months of 1995. Figure 4 shows WIND spacecraft observations of the 0.08–0.16 MeV/amu C+N+O (CNO) intensity, the solar wind speed and the magnetic field strength at 1 AU for approximately two and a half solar rotations in 1995. The particle intensity was

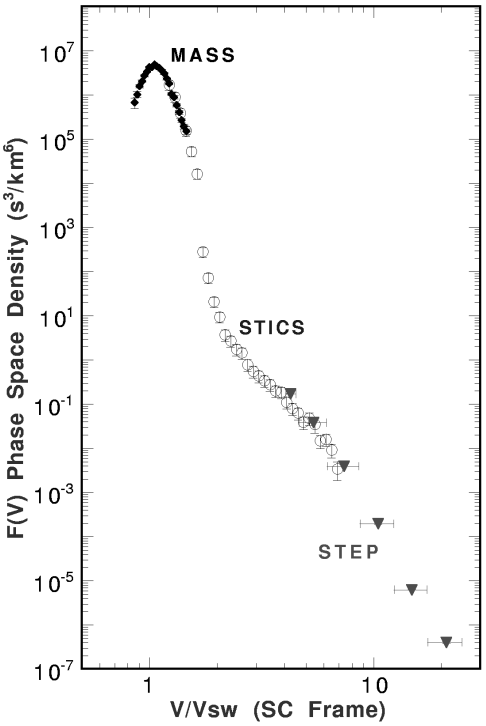

Figure 5. The helium phase space density *vs.* the particle speed with respect to the solar wind speed for the period 1995 day 150.4167–150.9375, using data from the MASS, STICS and STEP instruments onboard WIND. The CIR spectrum is an approximate power law down to energies where it merges smoothly with the solar wind.

measured by the STEP instrument (von Rosenvinge *et al.*, 1995), the solar wind data by SWE (Ogilvie *et al.*, 1995), and the magnetic field data by MFI (Lepping *et al.*, 1995). In Fig. 4, several high speed solar wind streams are visible, associated with enhancements in both the energetic particles and the magnetic field strength (compression regions). The arrows in the top panel, at April 7, 1995, (day 97) and May 30, 1995, (day 150), indicate two of the most intense CIRs observed by WIND since launch. Coronal hole maps from the National Solar Observatory, Kitt Peak (Solar Geophysical Data) indicate that these two CIRs are the same high speed wind structures, two solar rotations (54 days) apart.

With the exception of a small shock at 1995 day 97.84, the forward and reverse shocks usually have not yet formed at 1 AU (Hundhausen and Gosling, 1976). Nevertheless, as can be seen in Fig. 5, the energy spectrum for the time period 1995 day 150.4167–150.9375, during the most intense part of the CIR, extends down as an approximate power law to very low energies and in fact merge smoothly with the solar wind (Chotoo, 1998; Chotoo *et al.*, 1999). Assuming a typical mean free path (0.1–1 AU), this energy spectrum implies that the particles could not have originated far from 1 AU since there is no roll-over in the particle intensities at low

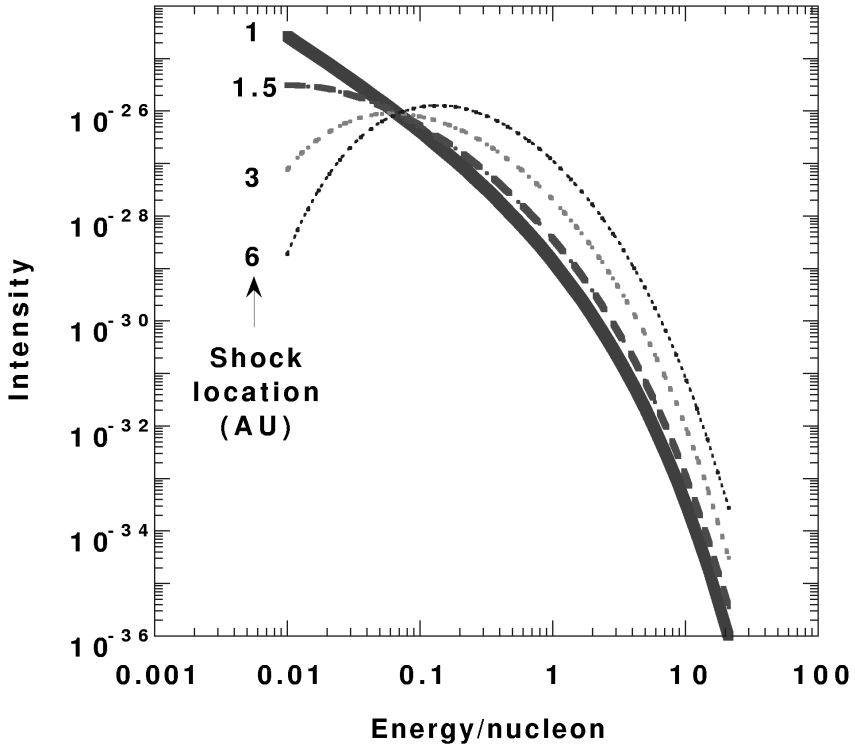

Figure 6. Energy spectra at 1 AU as predicted by the Fisk and Lee (1980) model for several source (shock) locations outside 1 AU. Note that in order for there to be no low energy roll-over, the source location must be near 1 AU.

energy. For example, using a jump in the magnetic field strength at the shock of 2.5, a particle mean-free path of 0.2 AU, and a solar wind speed of 800 km/s – all typical values – the analytical solution for the Fisk and Lee (1980) model shown in Fig. 6, is inconsistent with a power law below 0.1 MeV/amu ($V/V_{sw} \sim 5.5$) for a particle source inside about 1.5 AU.

Figure 7 shows the spectral indices measured at 0.2 MeV/amu of p, He, CNO, Ne through S (NeS), and Fe as functions of time for the most intense part of the May 30, 1995, CIR. Two features, which are typical of intense CIRs at 1 AU, are apparent: 1) for the same energy/amu, the temporal variation of the He, CNO, NeS, and Fe spectra are similar, despite having very different charge to mass ratios. 2) The energy spectra of all four groups of elements harden significantly with time. This hardening could either be a propagation effect or a change in the source spectra. As the CIR passes by, the spacecraft presumably becomes magnetically connected to increasingly distant regions of the CIR beyond 1 AU. If the low energy particles have smaller diffusion coefficients than high energy particles, because the particles must propagate upstream against the solar wind, a spectral hardening will

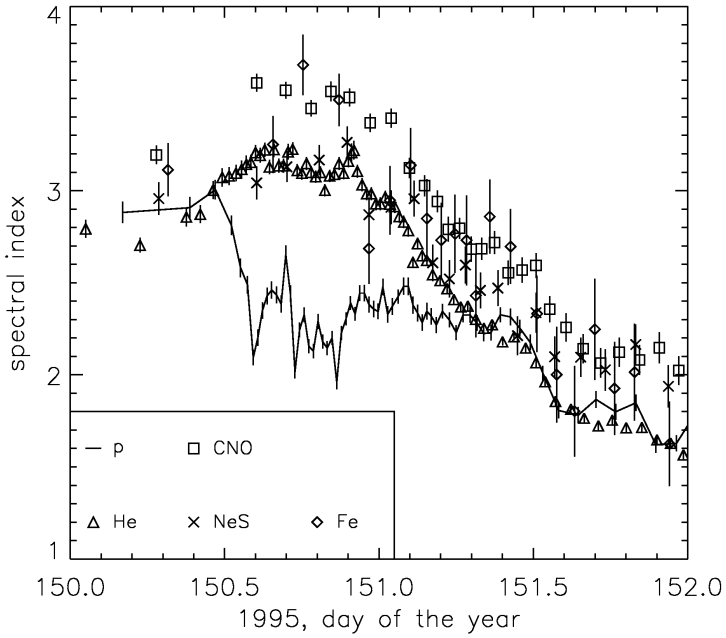

Figure 7. Spectral index at 0.2 MeV/amu *vs.* time for protons, helium, carbon+nitrogen+oxygen (CNO), neon through sulfur (NeS), and iron.

result since the low energy particles intensities fall off faster than the high energy intensities.

The proton spectra, as seen in Fig. 7, show a quite different time profile than that of the heavier elements. Dwyer *et al.* (1999) analyzed the proton data for several CIRs, including the May 30, 1995, CIR, and found that, unlike the heavy nuclei, the protons streamed radially outward (in the solar wind frame) and therefore were produced inside 1 AU. The outward flowing protons were also observed during the April 7, 1995, particle enhancement, which was the same CIR structure as the May 30, 1995, event, two solar rotations apart, suggesting that this additional proton component was associated with the CIR. Additional observations will be required in order to establish whether or not this behavior of protons is seen routinely.

5. Spectra: Temporal and Radial Evolution

R. B. DECKER, M. I. DESAI, and G. M. SIMNETT

5.1. ULYSSES OBSERVATIONS OF CIR PROTONS

While exploring the mid-latitude southern heliosphere from 13°S to 41°S during 1992 and 1993 (Marsden *et al.*, 1996), the Ulysses spacecraft encountered well-developed CIRs that were typically bounded by forward and reverse shocks on their

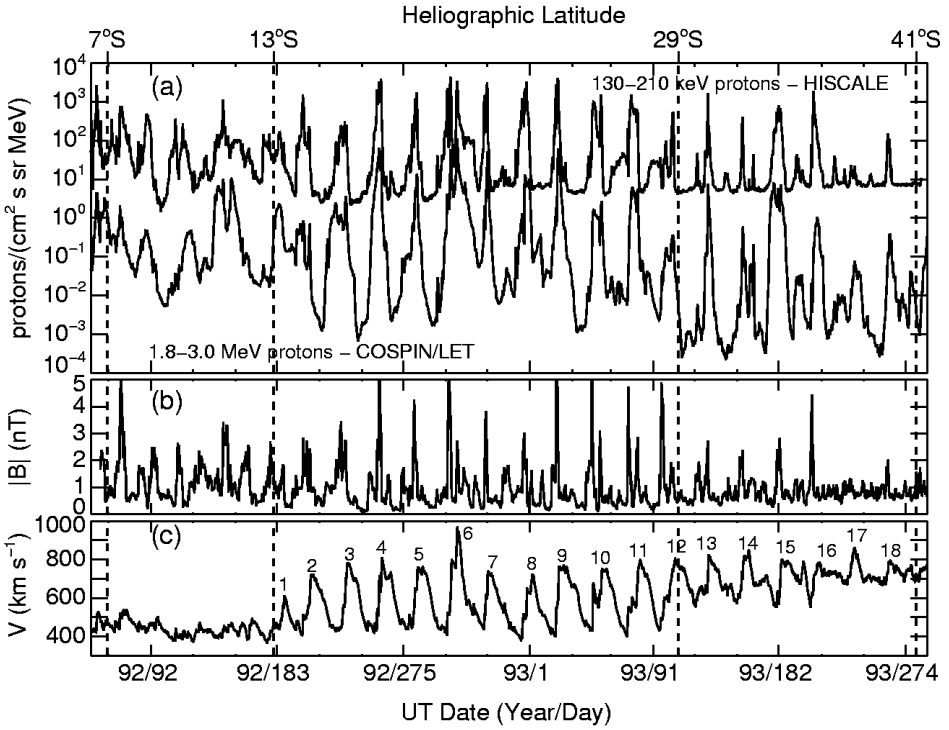

Figure 8. Overview of the Ulysses mission from day 48, 1992, to day 286, 1993, showing 6-hour averages of (a) the 130–210 keV (upper trace) and the 1.8–3.0 MeV (lower trace) proton intensities measured by HI-SCALE and COSPIN/LET, respectively, (b) the magnetic field magnitude, $|B|$ and (c) the solar wind speed, V. The dashed vertical lines demarcate the morphologically distinct regions, from the perspective of the CIR-related measurements, that Ulysses encountered in the southern heliosphere (see text and Sanderson *et al.* (1994)). The upper x-axis in panel a shows the heliographic latitude of Ulysses as a function of time. The numbers 1–18 in panel c refer to the appearance of the fast ($\sim$750 km/s) solar wind stream at Ulysses once every $\sim$26 days (after Bame *et al.*, 1993).

leading and trailing edges, respectively (Gosling *et al.*, 1993b). Figure 8 provides an overview of the Ulysses measurements of (a) the energetic proton intensities measured by HI-SCALE (130–210 keV) and COSPIN/LET (1.8–3 MeV), (b) the magnetic field magnitude, $|B|$, and (c) the solar wind speed, V, from day 48, 1992 to day 286, 1993. These CIRs were observed over 18 successive solar rotation periods (identified by the numbers 1–18 in Fig. 8c, after Gosling *et al.*, 1993b), and were formed due to the interactions between high-speed ($\sim$750 km/s) solar wind streams that emanated from the equatorward extension of the southern polar coronal hole and the slow speed ($\sim$400 km/s) flow of the streamer belt (Gosling *et al.*, 1993b). Figure 8a shows that the majority of the recurrent proton intensity increases coincided with the arrival of these CIRs. The principal findings of various charged particle instruments on board Ulysses during this period may be found in Sanderson *et al.* (1994), Simnett *et al.* (1994), and Desai *et al.* (1997; 1998).

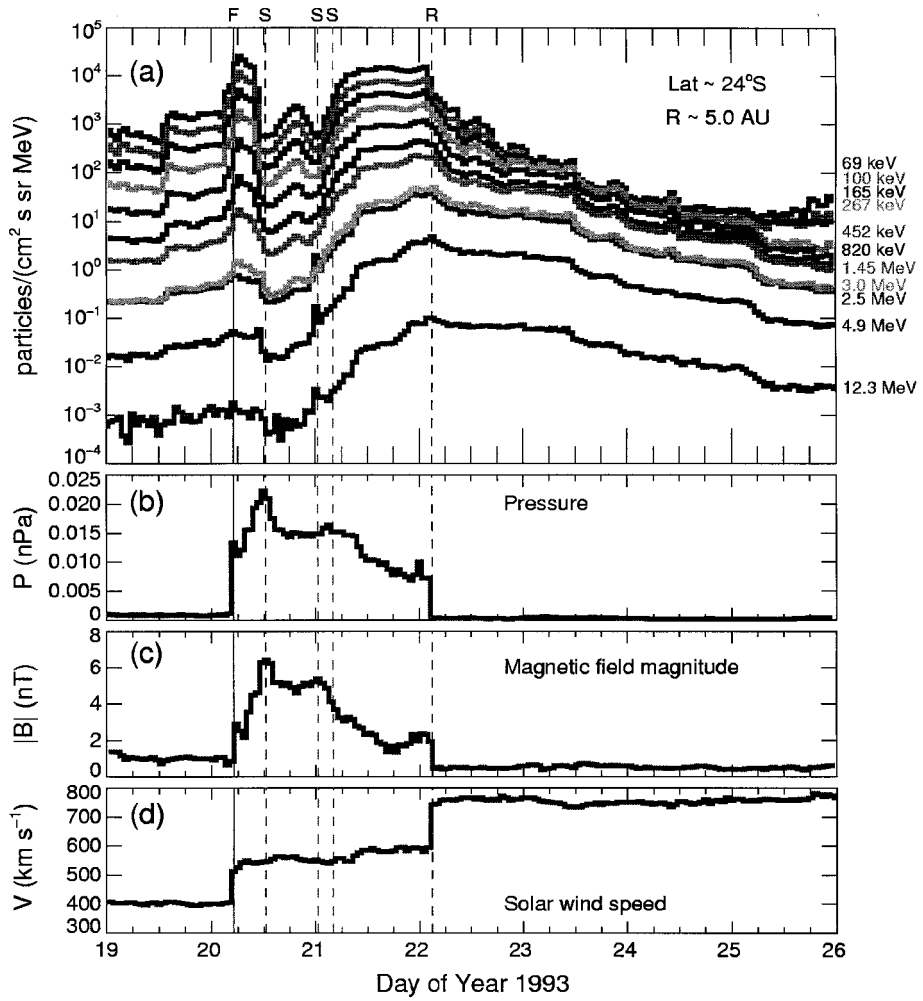

Figure 9. Hourly averages of (a) the 50-keV to 20-MeV proton intensities measured by HI-SCALE and COSPIN/LET, (b) the pressure, P, (c) the magnetic field magnitude, $|B|$, and (d) the solar wind speed, V, from day 19, 1993, to day 26, 1993. The intensity measured in each of the 11 discrete energy channels is denoted by the geometric mean of the upper and lower energy bounds of that channel. The solid (marked F) and dashed (marked R) vertical lines denote the times of arrival of the forward and the reverse shock, respectively (Gosling *et al.*, 1993b). The red vertical traces, marked S, denote the arrival times of the stream interfaces (see Wimmer–Schweingruber *et al.*, 1997, and the accompanying paper by Crooker, Gosling *et al.*, 1999).

Figure 9 shows the key features of CIR 9 (1993, days 19 to 26) from the perspective of hourly averaged measurements of (a) 50-keV to 20-MeV proton intensities obtained by HI-SCALE and COSPIN/LET, (b) the pressure, P, (c) the magnetic field magnitude, $|B|$, and (d) the solar wind speed, V. The location of Ulysses is given in Fig. 9a. The pressure P in Fig. 9b is given by the sum of the plasma and magnetic field pressures, *i.e.*, $P = 2n_{\mathrm{p}}kT_{\mathrm{p}} + B^2/2\mu_0$ where n_{p} and T_{p} are the proton

density and temperature, respectively, and $|B|$ is the magnetic field magnitude. Note that P does not specifically include the contribution of solar wind α particles and electrons.

Figure 9 shows that the leading and trailing edges of CIR 9 were bounded by a forward shock (marked F) and a reverse shock (marked R) that were observed at 0459 UT on day 20, 1993 and at 0257 UT on day 22, 1993, respectively. These shocks were identified by Gosling *et al.* (1993b) and Balogh *et al.* (1995) due to the abrupt increases in V (Fig. 9d) that were accompanied by simultaneous increases (at F) and decreases (at R) in P (Fig. 9b) and $|B|$ (Fig. 9c). We remark that CIR 9 was typical of the well-developed CIRs that were observed between 13° S and 29° S.

Figure 9a shows that the characteristics of the 50-keV to 20-MeV proton intensities are remarkably different at the forward and reverse shock of CIR 9. Specifically, the intensity increases above ∼500 keV near the reverse shock are substantially larger than those measured near the forward shock. Such differences have been observed previously in association with CIRs at Pioneer and Voyager (Barnes and Simpson, 1976; Tsurutani *et al.*, 1982; Decker *et al.*, 1981) near the ecliptic plane and at Ulysses (Desai *et al.*, 1998) throughout the three-dimensional heliosphere.

In contrast, the CIRs observed from 29° S to 41° S (see Fig. 8) were not bounded by local forward shocks while the reverse shocks and their associated proton intensity increases were weaker in comparison with the corresponding measurements obtained between 13° S and 29° S (Gosling *et al.*, 1993b).

5.2. Energy Spectra Observed at Ulysses

Figure 10 shows the 50-keV to 20-MeV proton energy spectra (solid circles) associated with the forward-reverse shock pair that bounded CIR 9 (see Fig. 9). Notice that the spectrum at the reverse shock (Fig. 10b) is much harder than the one at the forward shock (Fig. 10a), which once again exemplifies the differences between the particle observations near the leading and trailing edges of CIRs.

To test the CIR shock acceleration model of Fisk and Lee (1980), Desai *et al.* (1999) first fitted the 50-keV to 20-MeV proton differential energy spectra measured at all the corotating shocks observed at Ulysses with the functional form $j = j_0 v^{-n} \exp(-v/v_0)$, as predicted by the model. Here j is the differential intensity for a particle of velocity $v = \sqrt{E}$ (E is the energy of the particle in MeV), and the fit parameters j_0, n, and v_0 are the normalization constant, the spectral index, and the e-folding velocity, respectively. Notice that the fits (solid curves) to the spectra shown in Fig. 10 are excellent, both visually and statistically; $\chi^2_\nu \leq 2$ for $\nu = 8$ degrees of freedom.

Desai *et al.* (1999) then investigated the relationship between the fit parameters and various plasma and field parameters that characterize the strength of the shock. Figures 11a and 11b show the relationships between the spectral indices, n,

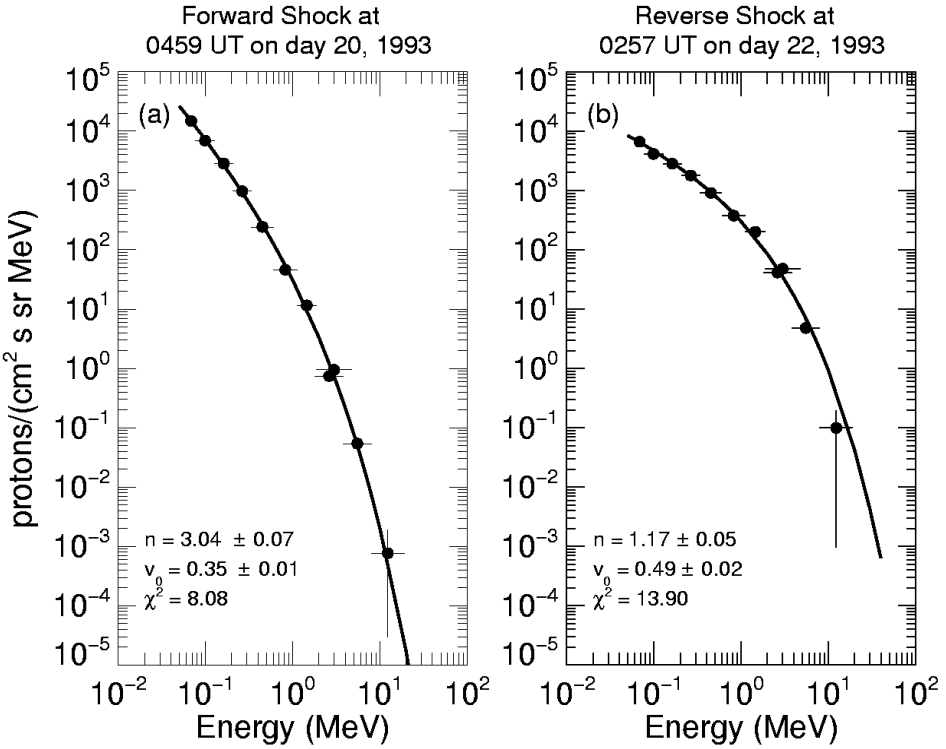

Figure 10. The differential energy spectra of 50-keV to 20-MeV protons measured by HI-SCALE and COSPIN/LET for the forward-reverse shock pair shown in Fig. 9. The spectra in panels a and b are derived from the average intensities measured from 0430 UT to 0530 UT on day 20, 1993 and from 0230 UT to 0330 UT on day 22, 1993, respectively. The solid curves represent the velocity function predicted by the Fisk and Lee (1980) model. The parameters n and v_0 denote the spectral index and the e-folding velocity, while the quantity χ^2 represents the goodness-of-fit statistic for each fit.

measured at the forward and reverse shocks, respectively and (1) the shock density compression ratio H (upper panels), (2) the heliographic latitude of Ulysses (middle panels), and (3) the plasma velocity $V_u' = V_{\rm sh} \sec \theta_{Bn}$ in the de Hoffman-Teller frame of the shock (lower panels); here $V_{\rm sh}$ is the shock velocity in the upstream plasma rest frame (Riley *et al.*, 1996), and θ_{Bn} is the shock normal angle (Balogh *et al.*, 1995).

The solid curves in the upper panels of Fig. 11 denote the relationship between n and H as predicted by the Fisk and Lee (1980) model (see the accompanying paper by Scholer, Mann *et al.*, 1999), while those in the middle panels are obtained by fitting cubic polynomials to the data. The dashed horizontal lines at $n = 2$ and $n = 1$ in the two upper panels are drawn to identify spectra with $n < 2$, *i. e.*, those spectra which, according to the Fisk and Lee (1980) model, should have been produced either by unphysical shocks with $H < 0$ or by shocks with $H > 4$ which are usually

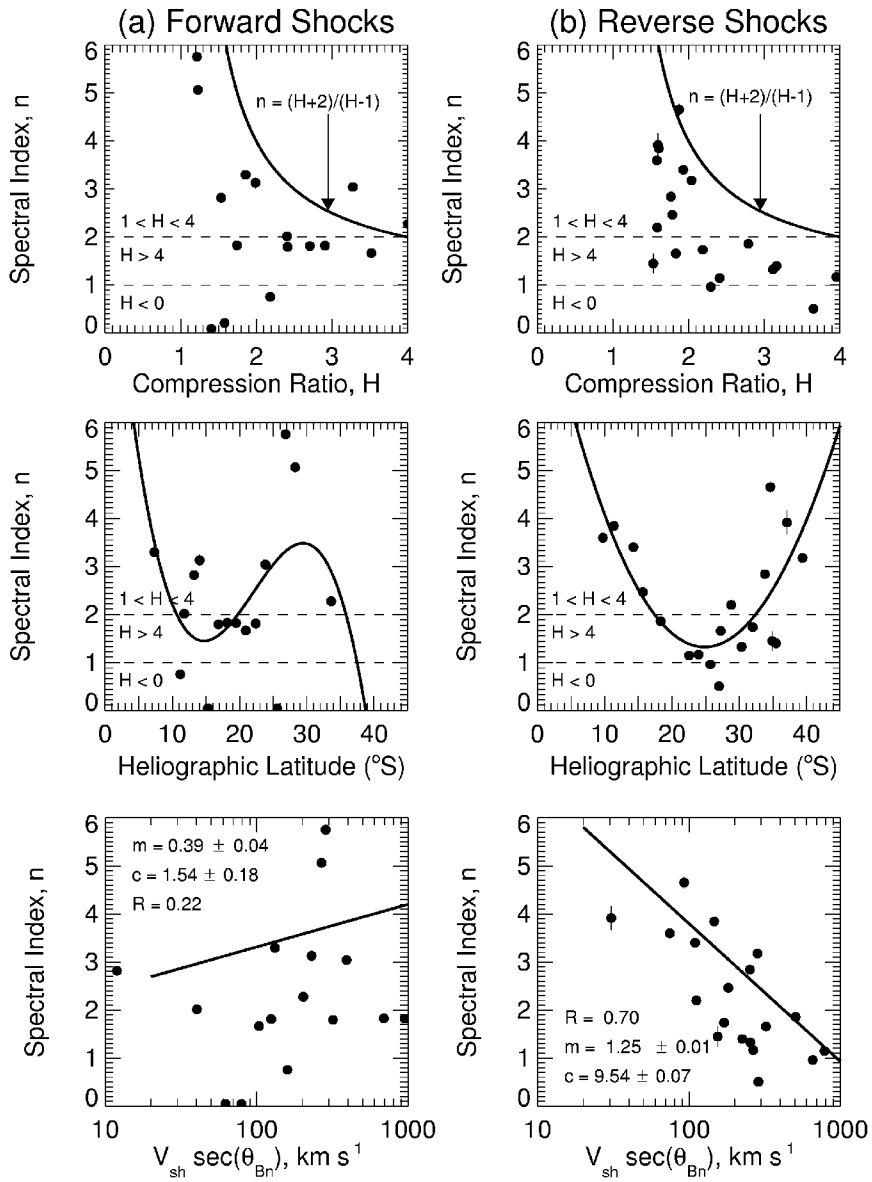

Figure 11. Relationship between the spectral index n measured at (a) the forward, and (b) the reverse shocks, and (1) the density compression ratio H (upper panels), (2) the heliographic latitude of Ulysses (middle panels), and (3) the plasma velocity $V_u' = V_{\rm sh} \sec \theta_{Bn}$ in the de Hoffman-Teller frame of the shock (lower panels). The solid curves in the upper panels represent the relation between n and H as predicted by the Fisk and Lee (1980) model, while those in the middle panels are obtained by fitting cubic polynomials to the data. The quantities m and c in the lower panels are the slopes and the intercepts, respectively, of the linear least squares fits (solid lines) to the data, and the quantity R denotes the linear correlation coefficients.

formed only in relativistic plasmas. The solid lines in the lower panels are linear least squares fits to the data.

The main results of Fig. 11 are as follows: (1) the relationships between the spectral indices and the shock compression ratio (upper panels) show significant departures from those predicted by the Fisk and Lee (1980) model; the observed spectra are substantially harder than predicted, (2) the spectral indices at the reverse shocks depend strongly on the heliographic latitude of Ulysses (middle panels); the hardest spectra are observed between 20° S and 30° S, (3) the spectral indices at the reverse shocks are anti-correlated with V_u' (lower panels); the hardest spectra are associated with strong quasi-perpendicular shocks, and (4) the spectral indices at the forward shocks show no dependence on either the shock parameters or the heliographic latitude.

In summary, the results of Desai *et al.* (1999) are inconsistent with the main predictions of the Fisk and Lee (1980) model. Desai *et al.* (1999) have suggested that the latitudinal dependence of the reverse shock spectra is probably related to the tilt ($\sim 25^\circ$) of the heliospheric current sheet with respect to the solar equatorial plane during 1992 and 1993. The negative correlation between the spectral indices at the reverse shocks and V_u' indicates that the gradient-drift mechanism plays a crucial role in accelerating particles at CIRs. The differences between the observations at the forward and reverse shocks may be due to the presence of both a more energetic seed population and an enhancement in the level of magnetic field fluctuations near the trailing edges of the CIRs. Desai *et al.* (1999) have suggested that these two effects are primarily responsible for increasing the efficiency of the acceleration mechanism at the reverse shocks.

5.3. VOYAGER 1 AND 2 FLUX PROFILES

By early 1999 the deep space probes Voyagers 1 and 2, launched in late 1977, reached respective heliocentric distances of 73 AU and 57 AU, heliographic longitudes 33° N and 20° S, and will be separated in longitude by only 35°. Their rectilinear separation will be nearly 75 AU. Each spacecraft carries a nearly identical set of instruments that continue to monitor plasma, field, and energetic particle activity in the outer heliosphere. We focus here on data from the LECP (Low Energy Charged Particle) instruments (Krimigis *et al.*, 1977) on the two spacecraft. The LECP instruments on Voyagers 1 and 2 measure the differential in energy fluxes and anisotropies of ions ≥ 30 keV and electrons ≥ 20 keV, the differential in energy ion composition ≥ 200 keV/amu, and the integral rates of cosmic ray protons > 70 MeV. Data acquired by these instruments during the past 21 years represent two-point measurements of energetic particle activity over separations in heliocentric distance up to 16 AU and in heliolatitude up to 53°.

Recurrent increases in the fluxes of ions with energies from at least 30 keV to several MeV are clearly evident in the LECP data throughout the Voyager missions (Hamilton *et al.*, 1978; Decker *et al.*, 1981; Gold *et al.*, 1986; 1988; 1991; Kane

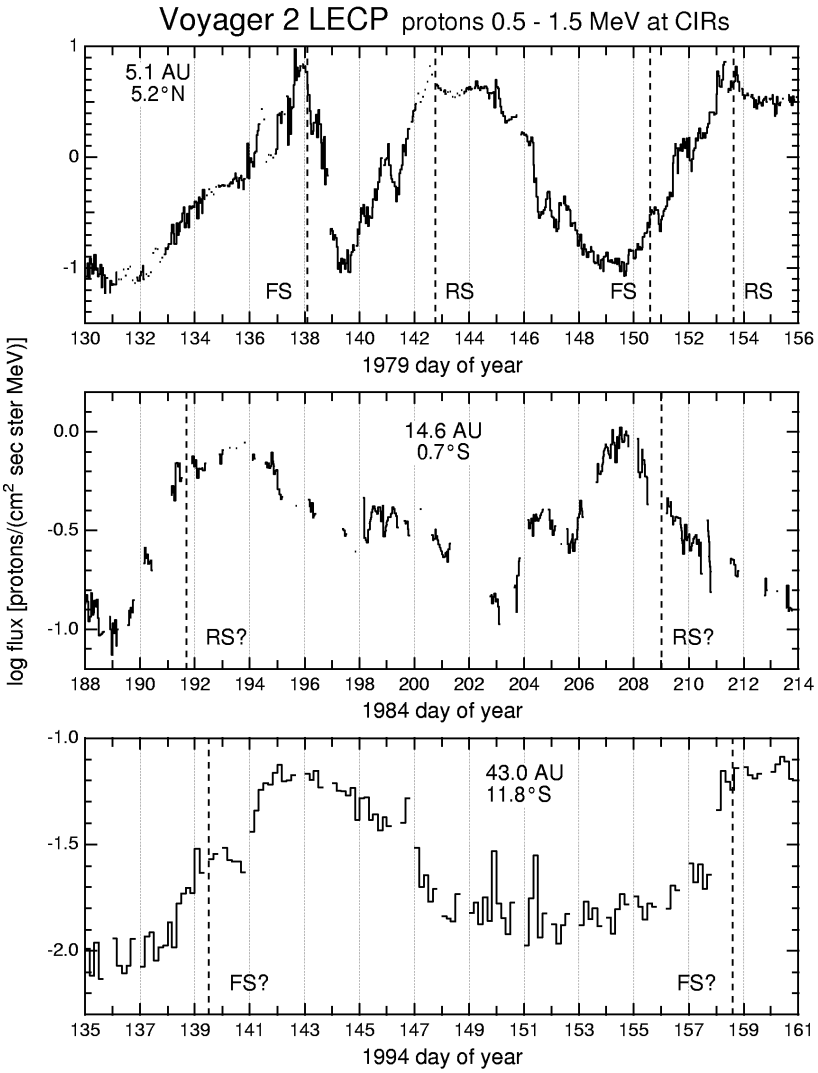

Figure 12. Fluxes of 0.52–1.45 MeV protons associated with CIRs during 1979 at 5 AU (top), during 1984 at 15 AU (middle), and during 1994 at 43 AU (bottom).

et al., 1995; Krimigis *et al.*, 1997; Lazarus *et al.*, 1999). Figure 12 shows three examples of CIR-associated flux increases of protons 0.52–1.45 MeV measured by the LECP on Voyager 2 during 1979 at 5.1 AU (pre-Jupiter), during 1984 at 14.6 AU, and during 1994 at 43 AU. Each panel contains 26 days of data, with data in the top two panels at 1-hour resolution, and those in the bottom panel at 6-hour resolution. The data acquisition rate and telemetry coverage were high during the 1979 period in preparation for Jupiter encounter in July, so the data quality is exceptionally good; however, data coverage in the 1984 and 1994 panels

is more representative of that available between planetary encounters and during the Voyager interstellar mission (*i. e.*, 1998-onward).

There were two forward-reverse shock pairs, as discerned from the Voyager 2 plasma science (PLS) data, during the solar rotation represented in the 1979 example period (Fig. 12, top panel). After a steady six-day build-up, the proton flux peaks near passage of the first forward shock (FS), a ∼100-fold increase above the ambient flux, decreases rapidly in the post-FS flow to a minimum in the center of the CIR, rises in the post-shock flow of the reverse shock (RS), peaks at the RS, and maintains a ∼2-day plateau upstream of the RS before declining steadily for ∼5 days back to a minimum on day 149. The second FS has little if any effect on the proton flux, and the flux-time profile at the second RS is basically a carbon copy of that associated with the first RS.

The example shown during the 26-day period of 1984 (Fig. 12, middle panel) illustrates the usefulness of the relatively broad energetic particle flux-time profiles as 'markers' for the presence of a nearby FS or RS even when frequent tracking gaps preclude the identification of the shocks in the high-resolution plasma and/or magnetic field data. Examination of the plasma and magnetic field data suggests that shocks may have passed the spacecraft sometime within the gaps, labeled 'RS?', but verification of a shock passage is not possible. However, the characteristic flux variations of energetic particles, such as those shown here, are reliable 'remote' signatures of a recent or impending shock passage. Note that at ∼15 AU, ∼1 MeV protons associated with acceleration at CIR shocks have peak fluxes ∼1 [in units of protons/(cm^2 s sr MeV)], whereas at ∼5 AU peak fluxes are ∼10. This is consistent with a decrease in peak fluxes of CIR-associated ion events as r^{-2}, where r is heliocentric distance, as reported by (Decker *et al.*, 1995), based on 30 to 4000 keV ion fluxes using Voyager 2 LECP data from early 1978 (4 AU) through 1994 (45 AU).

The bottom panel of Fig. 12 shows two CIR-associated proton flux increases at 43 AU. The question marks on the dashed vertical lines labeled 'FS?' now refer to possible shock-like structures. The structures are marked by rapid rises in plasma flow, but these rises are not as sharp as expected for shocks, and in addition the plasma density variations are not consistent with those of previously observed interplanetary shocks (Lazarus *et al.*, 1999). In any case, it is clear that these magnetohydrodynamical structures, classical collisionless shocks or not, are closely associated with flux increases of ions from at least 30 keV to several MeV. Ion acceleration either within the sharp flow velocity gradient, or in the enhanced turbulence in the near upstream and downstream regions of these structures must be occurring.

5.4. VOYAGER 1 AND 2 SPECTRA

Figure 13 shows 5-day averages of fluxes for four ion channels of Voyager 2 (left panel) and Voyager 1 (right panel) during the period 1983.7–1985.5. This period

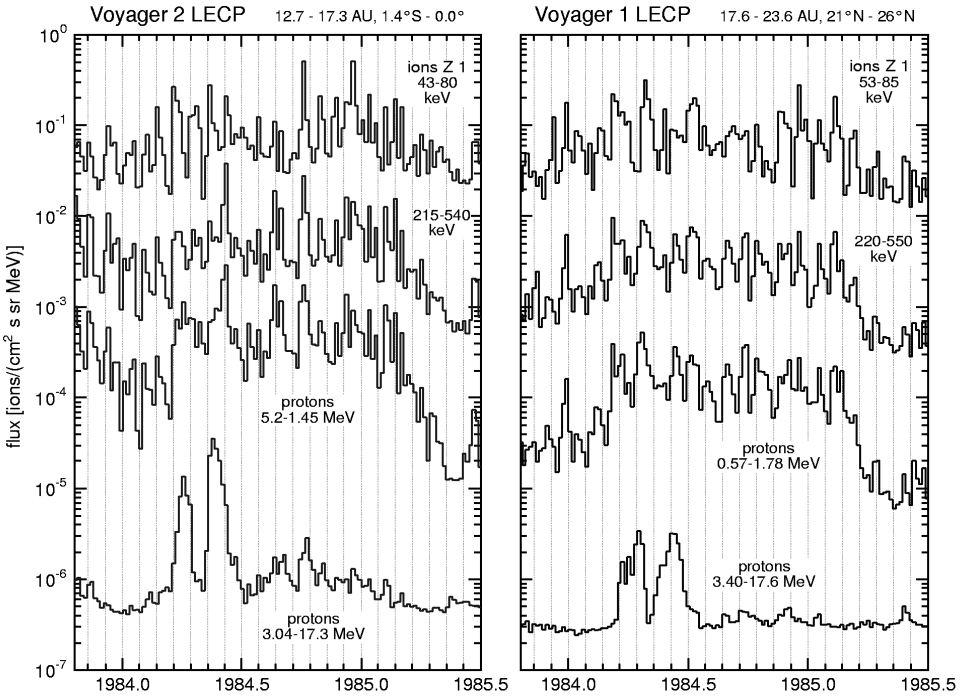

Figure 13. 5-day averages of low-energy ion fluxes at Voyager 2 (left) and Voyager 1 (right) during CIR-dominated period 1984 to first quarter of 1985.

is of interest not only because the ion fluxes were dominated by CIR shock acceleration, but also because Voyager 2 was near the heliographic equator and at ∼13–17 AU, while Voyager 1 was at ∼23° N heliographic latitude and at 18–24 AU. There were two major injections of solar energetic particles in 1984 (note the 3–17 MeV channels), but these periods were not used when CIR-associated energy spectra were calculated.

It has been argued that the striking 26-day recurrent energetic ion and electron flux variations observed at Ulysses above ∼30° S latitude during its southbound pass are particles accelerated at low latitudes at CIR shocks at ∼15–20 AU (Simnett and Roelof, 1997; Fisk and Jokipii, 1999). These source particles must propagate radially inward and to high latitudes to be subsequently observed at Ulysses. The Voyager observations in Fig. 13 represent the ion 'source function,' albeit a solar cycle earlier, that one might adopt to model (*e. g.*, cross-field diffusion, Fisk-field transport, etc.) the high-latitude Ulysses observations.

Figure 14 shows energy spectra of $Z \geq 1$ ions with energies 43–3500 keV observed during 1979, 1984, and 1994 at Voyager 2. Each spectrum represents the average over the peak fluxes for several recurrent events observed during the respective year. The 1984 spectrum is the 'source function' discussed above. Note that the shape of the spectrum is maintained over a large radial range (∼40 AU)

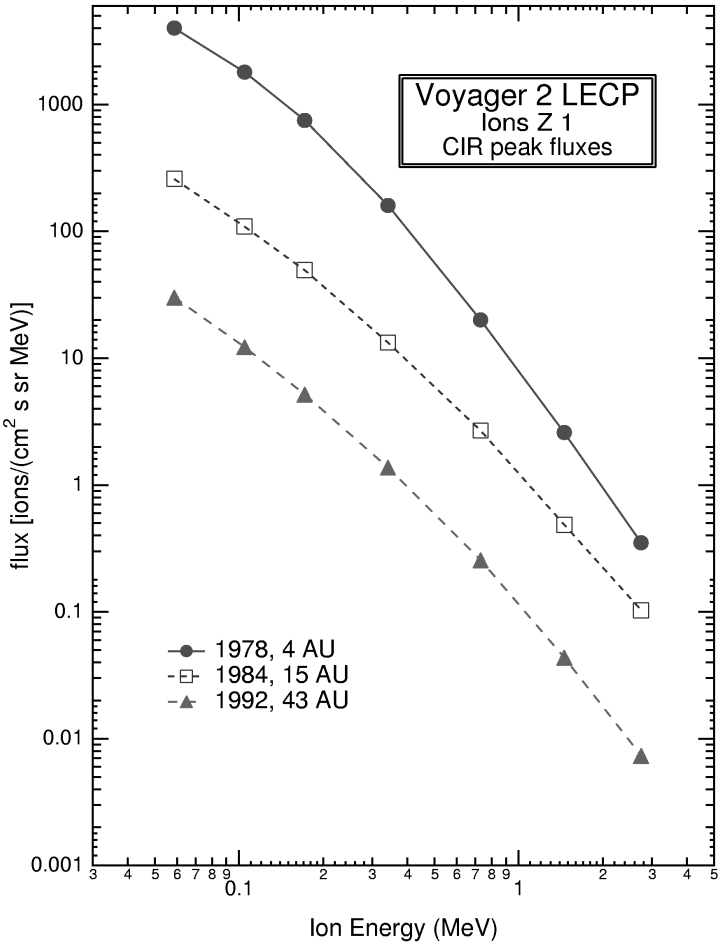

Figure 14. Energy spectra of $Z \geq 1$ ions 43–3500 keV during peak fluxes at CIR-associated events at Voyager 2 in 1979 (4 AU), 1984 (15 AU), and 1994 (43 AU).

and time (1.5 solar cycles). It is not clear why the energy spectrum has this form, and why this form is an approximate invariant with respect to heliocentric distance. This spectral form is also observed in the Voyager 1 LECP ion data (40–4000 keV) at $\sim 30^{\circ}$N. It remains a theoretical challenge to explain how this energy spectrum is produced in the vicinity of corotating shocks and why the spectral form is insensitive to large variations in heliocentric distance and heliolatitude.

5.5. DISTANT HELIOSPHERE

In the distant heliosphere, CIR fluxes continue to evolve, forming global structures with long lifetimes. Details of the outer-heliospheric properties are discussed in the accompanying paper by Gazis, McDonald *et al.* (1999).

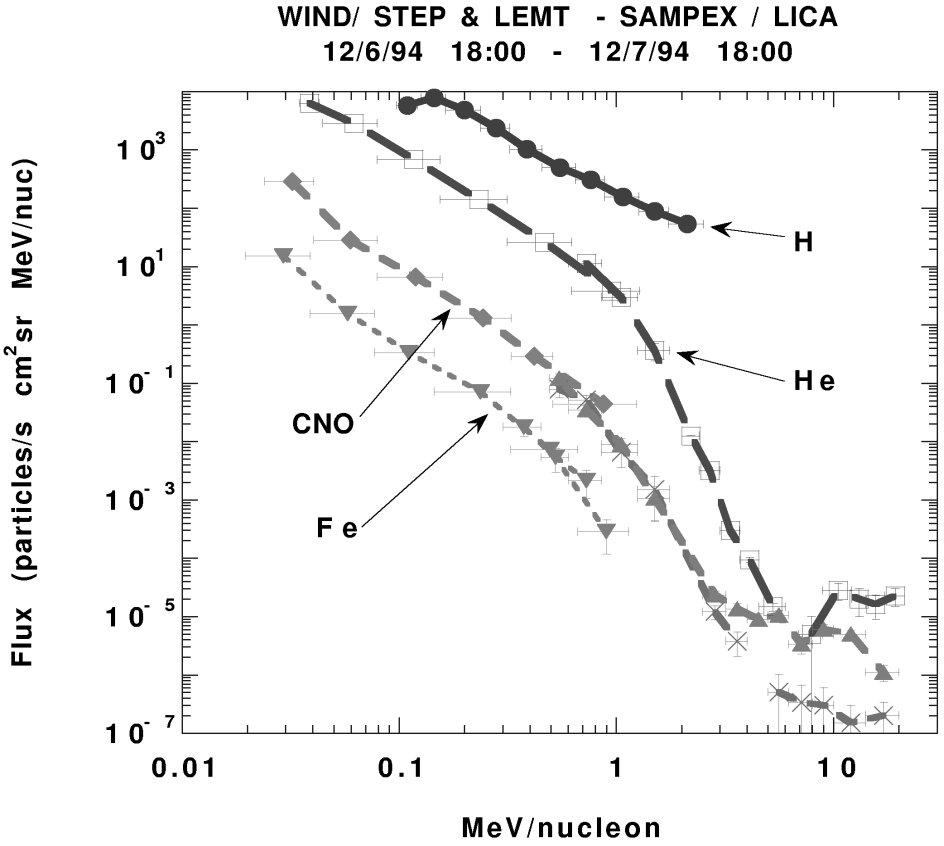

Figure 15. Energy spectra for the 24-hour period starting Dec. 6, 1994 1800 UT. Note power law spectra at low energies, rolling over above ∼1 MeV/amu.

6. Composition: Averages, Time Variations; Radial and Latitude Variations

G. M. MASON, G. GLOECKLER, M. HILCHENBACH, R. KALLENBACH, and E. KEPPLER

The accompanying paper by Mason and Sanderson (1999) summarized CIR properties reported in the years before the Ulysses and WIND missions. In this section we summarize new compositional features observed due to advances in instrumentation or to the unique trajectory of Ulysses.

6.1. ION COMPOSITION

Figure 15 shows energy spectra during a 24-hour period near the peak of the December 6, 1994, CIR, as measured with the EPACT/STEP and LEMT instruments on the WIND spacecraft (Mason *et al.*, 1997). These spectra are typical of CIRs ob-

TABLE III
Energetic particle abundances normalized to O observed in CIRs 1992–1995

	STEP[1] 150 keV amu^{-1}	LICA[2] 1 MeV amu^{-1}	SW coronal hole[1]	SW in ecliptic[3]	SW average low + high	STEP/ SW average low + high	LICA/ SW average low + high
H	907±444		1590±500	1900± 400	1745±320	0.52±0.27	
He	113±20	211±17	83±25	75±20	79±16	1.43±0.39	2.67±0.58
C	0.75±0.12	0.94±0.07	0.70±0.10	0.72±0.10	0.71±0.07	1.05±0.20	1.33±0.17
N	0.15±0.04	0.15±0.01	0.13±0.01	0.14±0.01	1.09±0.27		
O	≡ 1.	≡ 1.	≡ 1.	≡ 1.	≡ 1.	≡ 1.	≡ 1.
Ne	0.21±0.05	0.17±0.02	0.14±0.01	0.14±0.02	0.14±0.01	1.53±0.41	1.24±0.17
Mg	0.13±0.03	0.10±0.02	0.08±0.02	0.16±0.03	0.12±0.02	1.05±0.27	0.81±0.17
Si	0.11±0.02	0.08±0.01	0.05±0.01	0.19±0.04	0.12±0.02	0.91±0.25	0.66±0.15
S	0.03±0.01	0.02±0.00	0.04±0.01	0.03±0.00	0.98±0.32		
Fe	0.08±0.03	0.10±0.01	0.06±0.01	0.12±0.03	0.09±0.02	0.89±0.42	1.07±0.23

[1] Average of 5 events between December 1992 and October 1994
[2] Average of 12 events between November 1994 and July 1995
[3] von Steiger *et al.* (1997), their table 1

served on WIND during 1994 and 1995. Note that below ∼1 MeV/amu the spectra of H, He, C+N+O, and Fe are all power laws that continue down to the instrument threshold near 30 keV/amu. Indeed, for Helium, which can be measured down to solar wind energies by the WIND/STICS instrument, the spectrum remains a power law to even lower energies as already shown in Fig. 5 (Chotoo, 1998; Chotoo *et al.*, 1999). Above 1 MeV/amu, the spectra in Fig. 15 steepen significantly, and then finally exhibit a "bump" around 10 MeV/amu due to anomalous cosmic ray He and O.

Table III lists energetic particle abundances normalized to O observed in a series of CIRs from 1992 through 1995 (Mason *et al.*, 1997), and compares them with recent solar wind plasma measurements from Ulysses (von Steiger *et al.*, 1997). As has been known from prior work, there is a general similarity between energetic particle CIR abundances and solar wind abundances, although some puzzling differences exist for He, C, and Ne. Recent observations on Ulysses have revealed systematic differences in the composition of slow *vs.* fast solar wind streams, wherein the fast streams showed reduced enhancements of elements with low First Ionization Potential (FIP) compared with the slow streams. This can be seen in Table III, for example, where the Mg and Fe abundances in the fast streams are about a factor of 2 less than in the slow streams (see also Wimmer–Schweingruber *et al.*, 1997).

In order to search for a similar effect in the energetic ion population, Mason *et al.* (1997) examined the Mg/O ratio during the passage of the intense May 30, 1995, CIR. In Fig. 16, the upper panel shows the 70 keV/amu O flux, and the bottom panel shows the 70 keV/amu Mg/O ratio. In the lower panel, the shaded area marks the

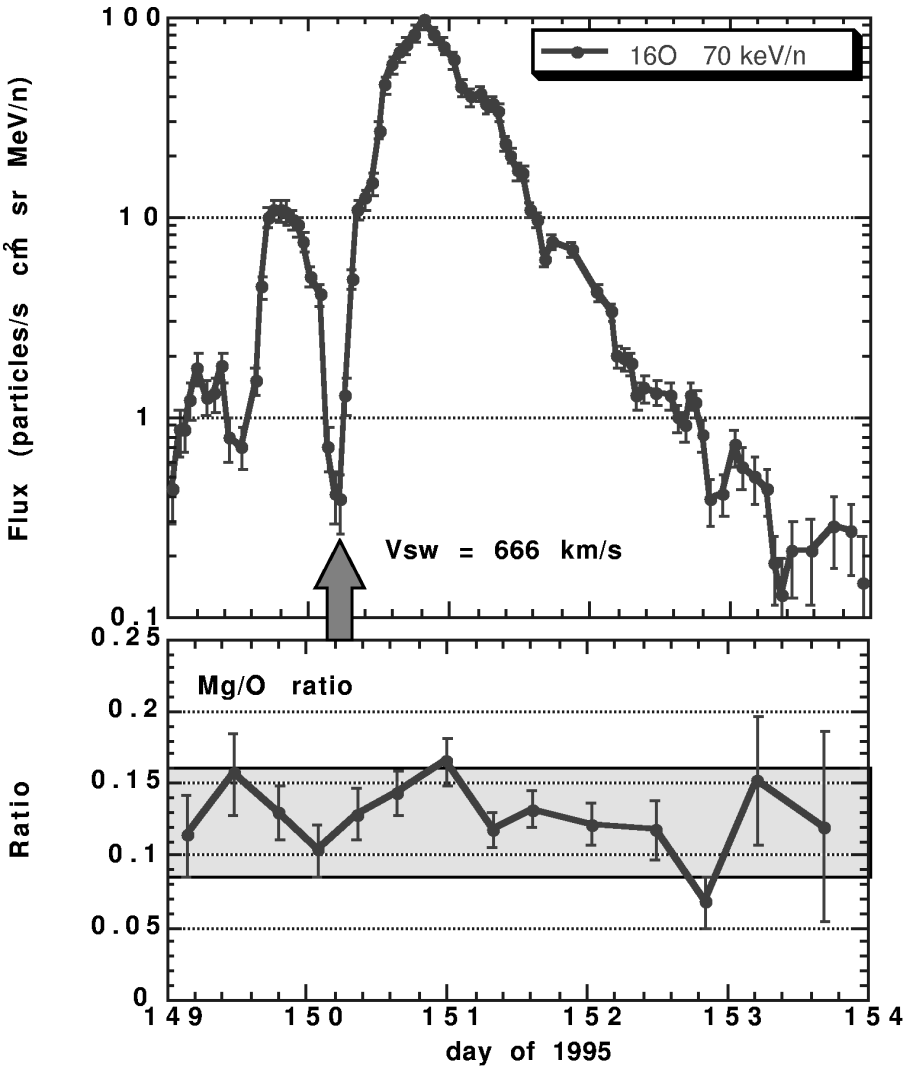

Figure 16. Top panel: Time-intensity profile of 70 keV/amu O fluxes during the CIR of May 30, 1995, measured on the WIND spacecraft. *Arrow* marks stream interface. *Lower panel:* 6-hour average Mg/O ratio at 70 keV/amu. Shaded area shows range of Ulysses solar wind Mg/O for slow solar wind (upper edge of box) and fast solar wind (lower edge of box). Average solar wind speed during this event was 666 km/s.

upper and lower bounds of the solar wind Mg/O ratio observed on Ulysses in slow *vs.* fast streams, respectively. The transition from slow to fast solar wind at stream interface (SI) passage occurred at day 150.18, and is marked with an arrow. For the energetic particles, the Mg/O ratio shows no particular trend during the CIR, but rather fluctuates around the middle of the shaded box, which is to say near the *average* of the Ulysses slow- and fast-stream values.

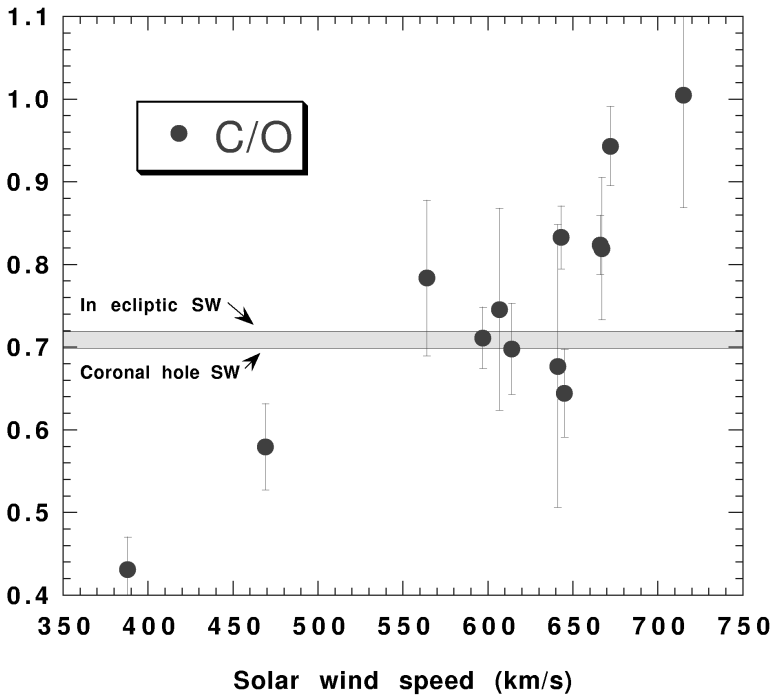

Figure 17. WIND spacecraft measurements in the energy range at around 150 keV/amu: Carbon to oxygen (C/O) abundance ratio in 12 CIRs *vs.* solar wind speed during the event. The shaded area shows the range of solar wind C/O abundance ratios observed in slow and fast solar wind streams.

Another newly discovered feature of CIR abundances is shown in Fig. 17, which displays the 150 keV/amu C/O ratio as a function of solar wind speed for 12 CIRs observed on WIND (Mason *et al.*, 1997). The shaded area shows the range of C/O ratios observed in fast and slow solar wind streams. Notice the strong increase of C abundance compared with O as the solar wind speed increases, rising from well below to well above the average solar wind speed value of 0.7 (von Steiger *et al.*, 1997).

This behavior was also reported for Ne/O, while other ratios such as He/O, Mg/O, and Si/O showed no dependence on solar wind speed. Note in this context that the C^+ pickup ion abundance in the inner heliosphere is strongly dominated by the so-called inner source (Geiss and Witte, 1996) and that He and Ne are the two elements of the interstellar neutral gas that penetrate deepest into the heliosphere. In the accompanying paper by Scholer, Mann *et al.* (1999) models are discussed which can explain why pickup ion abundances are enhanced by two orders of magnitude in the suprathermal particle populations associated with CIRs over the abundances of ions which originate from the solar wind.

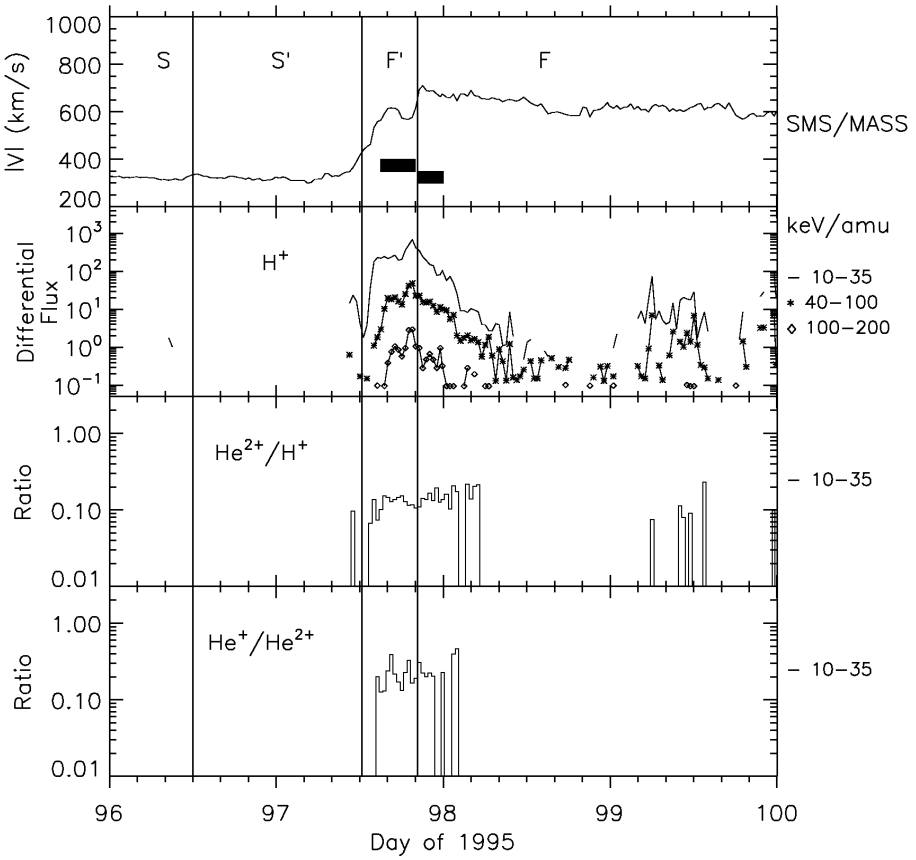

Figure 18. WIND spacecraft measurements of fluxes of low energy ions at 1 AU during the April 7, 1995, CIR. Top panel, solar wind speed; following 3 panels, H^+, He^{++}/H^+ ratio, and He^+/He^{++} ratio. Notice that the pick-up He^+ is about 20% of He, and is essentially constant in time.

6.2. Helium Charge States

An entirely new channel of CIR properties has been opened up by the advent of instruments capable of measuring CIR ion composition as well as the ionization states of the nuclei (Gloeckler *et al.*, 1992; 1995; Hovestadt *et al.*, 1995). Figure 18 shows several ion species observed on WIND during the April 7, 1995 CIR (Chotoo, 1998; Chotoo *et al.*, 1999). The upper panel of the figure shows the solar wind speed; the second panel the H^+ particle intensity in three energy ranges, the third panel the He^{++}/H^+ ratio from 10–35 keV/amu, and the bottom panel the He^+/He^{++} intensity from 10–35 keV/amu. Since singly ionized He is rare in the solar wind, its presence in the CIR energetic particles is most likely due to a pick-up ion source rather than solar wind (Gloeckler *et al.*, 1994; Chotoo, 1998; Chotoo *et al.*, 1999). The abundance of He^+ relative to He^{++} is $\sim$20% during this period.

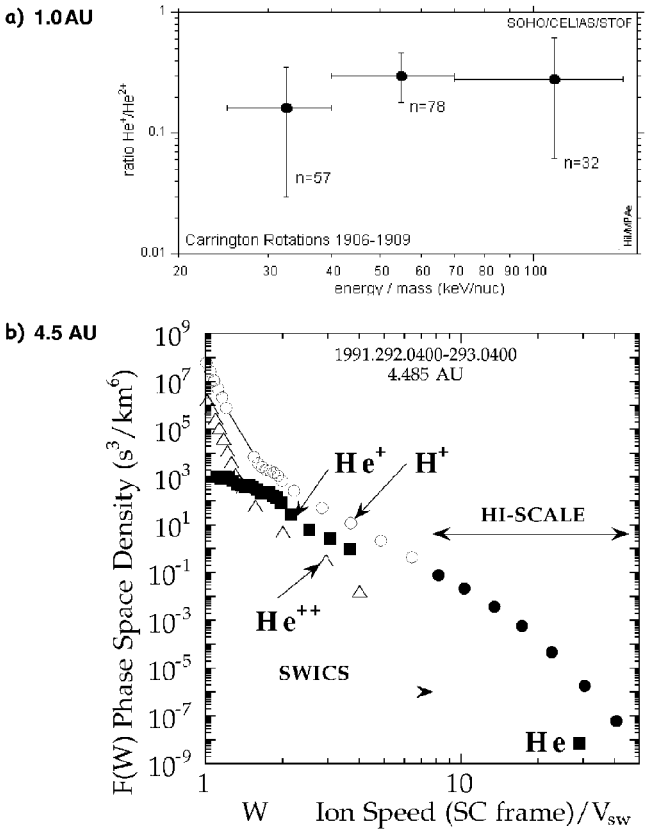

Figure 19. a) Ratio of pick-up He^+ to solar wind He^{++} as a function of energy as observed in a series of CIRs at 1 AU. b) CIR accelerated ions during the October 19, 1991 event observed by Ulysses at 4.485 AU. Note that pick-up He^+ exceeds the He^{++} by a factor of ∼2, in contrast to the observations at 1 AU in a) and in Fig. 18, where He^{++} dominates.

Figure 19a) shows the average He^+/He^{++} ratio in several CIRs observed on SOHO during Carrington Rotations 1906–1909 (Hilchenbach *et al.*, 1997). Over the energy range ∼30–120 keV/amu, this ratio is roughly 0.2, and shows no significant energy dependence. Thus, pick-up He^+ appears to be energized in CIRs, but at 1 AU it was nevertheless a minor component of the He abundance.

In contrast, Fig. 19b) shows He^+ and He^{++} spectra in the October 18–21, 1991 CIR observed at Ulysses at 4.5 AU (Gloeckler *et al.*, 1994). In the figure, the phase space density is plotted *vs.* the ion/solar wind speed ratio; since the solar wind speed during the period was about 400 km/s, the upper range of the He^+ data corresponds to about 15 keV/amu, or somewhat below the 1 AU observations shown in Fig. 18 and 19a). Nevertheless, the shape of the He^+ spectrum, and its similarity to the H^+ and He^{++} spectra suggests that it continues to higher energies and is a significant fraction of the energetic He observed by the HI-SCALE (Lanzerotti

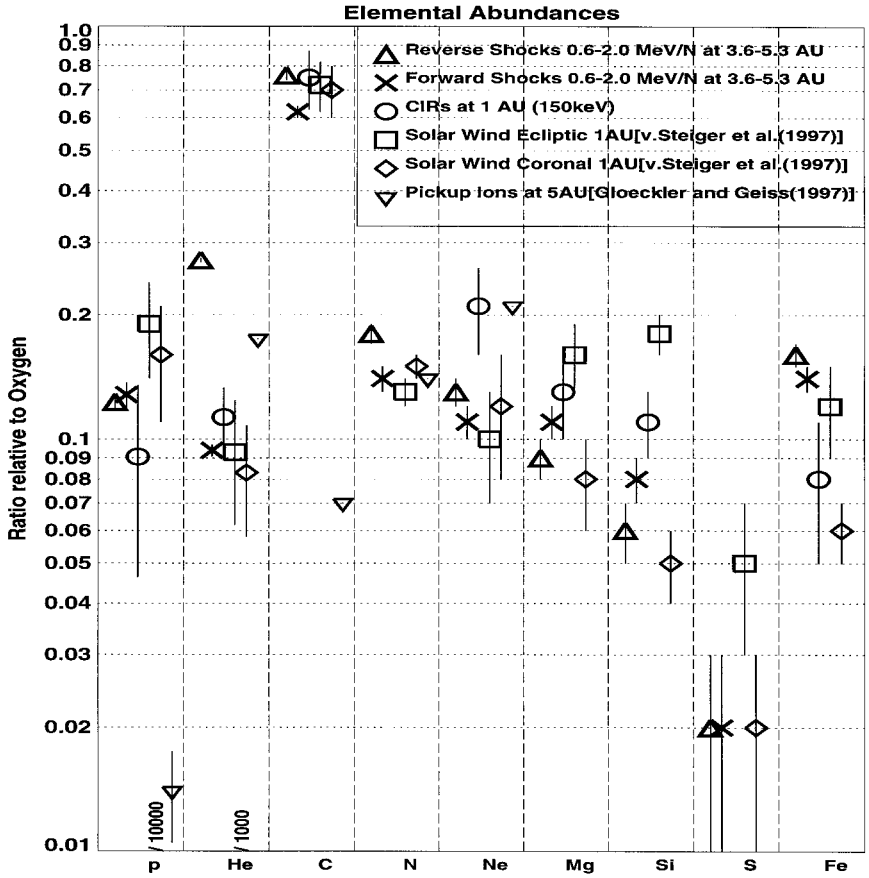

Figure 20. Ulysses energetic particle abundances at forward and reverse shocks (0.6–2.0 MeV/amu) compared with 1 AU observations at 150 keV/amu, normalized to O = 1. Note the differences in He abundance at 1 AU and at Ulysses.

et al., 1973) instrument out to energies of ∼1 MeV/amu (Gloeckler *et al.*, 1994). The fact that He^{+} is about twice as abundant as He^{++} at 4.5 AU, and yet is only about 15% of the total He observed near 1 AU is strong evidence that at these low energies, the CIR ions have difficulty moving into the inner heliosphere. This is consistent with the expectation of the Fisk and Lee (1980) model as shown in Fig. 6.

6.3. Radial and Latitude Evolution of CIR Ion Composition

Advanced instruments on the Ulysses mission make it possible for the first time to study a broad range of heavy ion composition in CIR ions at distances far beyond 1 AU (Keppler *et al.*, 1992; Lanzerotti *et al.*, 1992; Simpson *et al.*, 1992). Figure 20 compares Ulysses in-ecliptic data, along with out-of-ecliptic data with low energy ion abundances from 1 AU (Fränz *et al.*, 1999). From the figure it can be seen that all the minor species (C, N, Ne, Mg, Si, S, and Fe) show the same

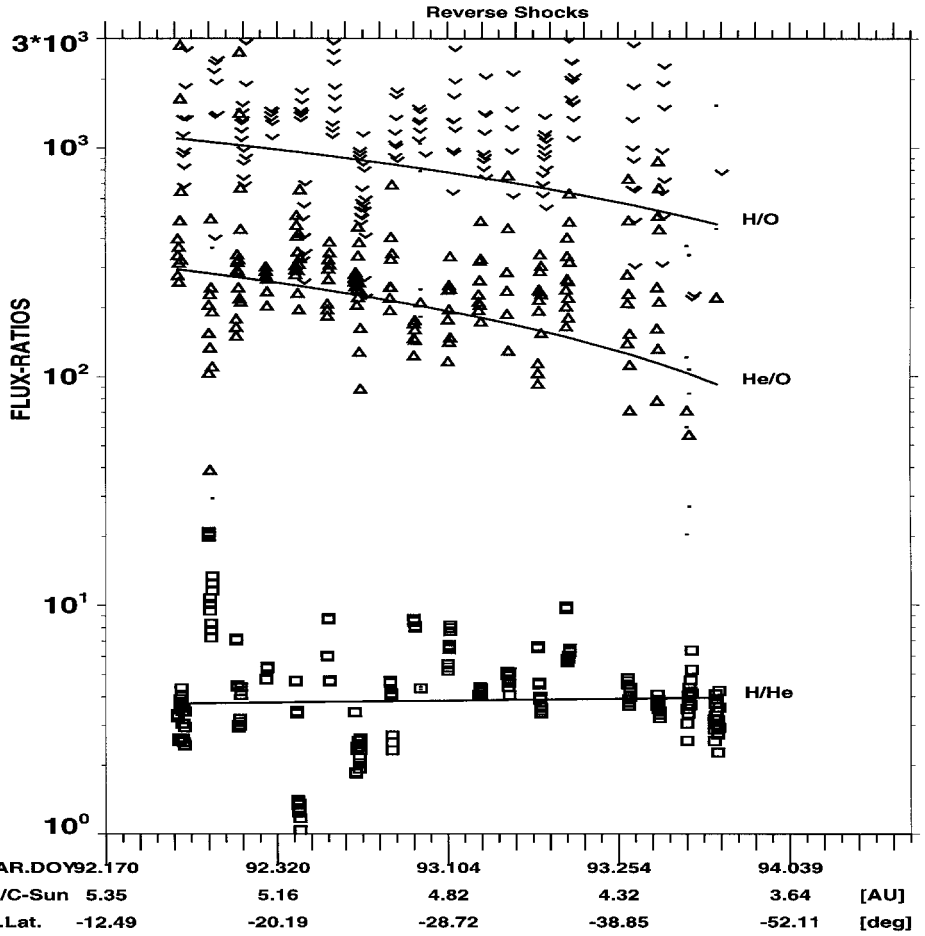

Figure 21. Temporal variation of the H/O, He/O and H/He ratios during reverse shock passages observed on Ulysses. On the plot, values at the left are at larger heliocentric distances and lower heliolatitudes.

abundance within two sstandard deviations during the forward and reverse shock periods. C, N, and Ne are overabundant by more than one standard deviation during the reverse shock periods. However, the most significant difference is seen for He, which has a ratio of 2.5 between the forward and reverse shock periods. Figure 21 shows the variation of 0.52–0.8 MeV/amu daily averages of H/O, He/O, and H/He in the reverse shock periods (Fränz *et al.*, 1999). Although the spread in the data is quite large, nevertheless there is evidence that the H/O and He/O ratios decrease as Ulysses moved away from the current sheet. Taking together the trends in Figs. 20 and 21, Fränz *et al.* (1999) conclude that at solar distances of 3–5 AU He pick up ions dominate the energetic He intensities, and that this acceleration occurs only at the CIR reverse shocks.

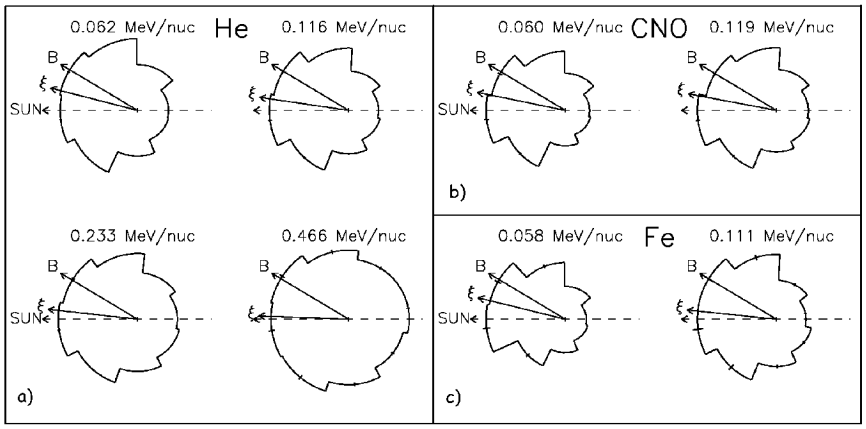

Figure 22. Energetic He (a), CNO (b) and Fe (c) intensities in the solar wind frame *vs.* azimuthal angle of the particle velocity in the ecliptic plane measured on the WIND spacecraft. The data are averaged over the time period 1995 day 150.6–151.0, following the stream interface during the most intense part of the CIR. Note that the direction of the first-order anisotropy, ξ, which indicates the flow direction of the particles, is in all cases directed sunward and is different from the magnetic field *B* direction.

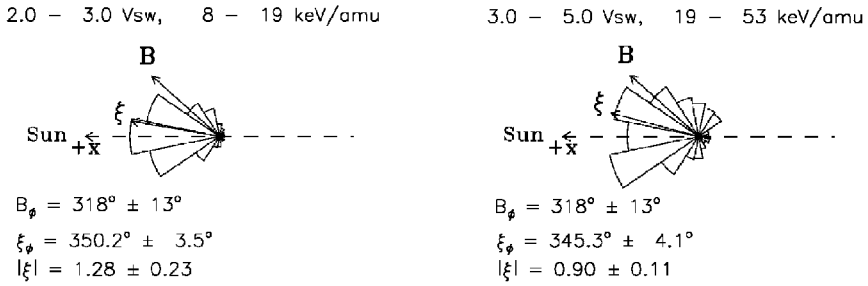

Figure 23. The helium intensities in the solar wind frame versus azimuthal angle (of the particle velocity) in the ecliptic plane as measured by the STICS instrument on WIND (Chotoo, 1998). The data are averaged over a 4-hour time period following the stream interface and centered at 1995 day 150.67. As with the STEP results shown in Fig. 22, the direction of the first-order anisotropy, ξ, is directed sunward and is different from the magnetic field *B* direction.

7. Anisotropies at 1 AU

J. R. DWYER

Figure 22 shows azimuthal plots of the He, CNO and Fe intensities, in the solar wind frame, in the $X - Y$ GSE plane for a 9.6 hour time period during the May 30, 1995, CIR, as observed on the WIND spacecraft at 1 AU. The sunward particle flow, in the solar wind frame, indicates a source beyond 1 AU and is consistent with a CIR origin of the particles. However, the CIR anisotropy is not directed along the average magnetic field line, implying substantial perpendicular transport as previously reported by Dwyer *et al.* (1999) for the three most intense CIRs observed by WIND. Figure 23 demonstrates that these results agree with measurements from

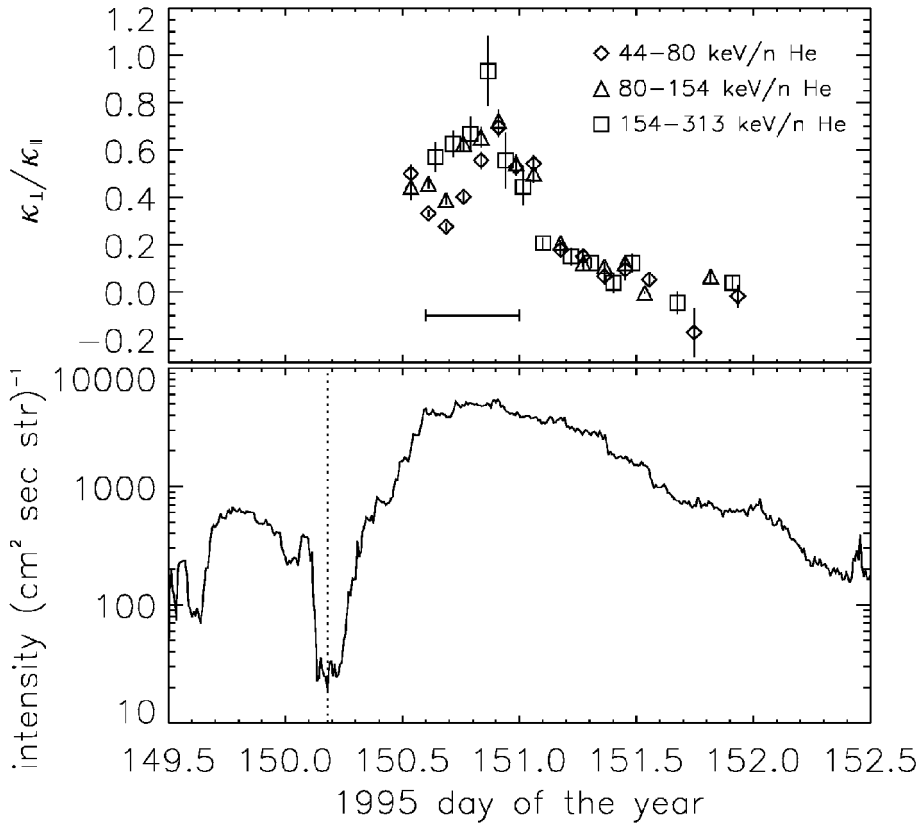

Figure 24. $\kappa_\perp/\kappa_\parallel$ versus time (top panel) for the May 30, 1995, CIR for three energies. $\kappa_\perp/\kappa_\parallel$ is calculated for each time period from the azimuthal angle of the particle anisotropy, φ_{ani}, and the magnetic field, φ_B, by assuming that the gradient direction is constant and φ_{grad}=180°. The bottom panel shows the 44–620 keV/amu helium intensity for the same time period. The dip in the helium intensity seen at day 150.2 coincides with the passage of the stream interface (dashed line). The horizontal bar shows the time period for this CIR used in Fig. 22. These observations are from the WIND spacecraft at 1 AU.

the STICS instrument (Gloeckler *et al.*, 1995), which also measured significant cross-field transport for extended periods of time during this CIR as well as the April 7, 1995, CIR (Chotoo, 1998; Chotoo *et al.*, 1999).

Using a simple diffusion model of particle transport, Dwyer *et al.* (1999) calculated the ratio of the perpendicular to parallel diffusion coefficients, $\kappa_\perp/\kappa_\parallel$ as a function of time during the May 30, 1995, CIR. As can be seen in Fig. 24, if the perpendicular transport observed by STEP is interpreted as due to particle diffusion then $\kappa_\perp/\kappa_\parallel$ must exceed 0.4 for almost 12 hours during the peak of the CIR. This ratio is significantly larger than values commonly found in the literature, suggesting that the role of perpendicular transport in the heliosphere and in many other astrophysical environments should be reexamined.

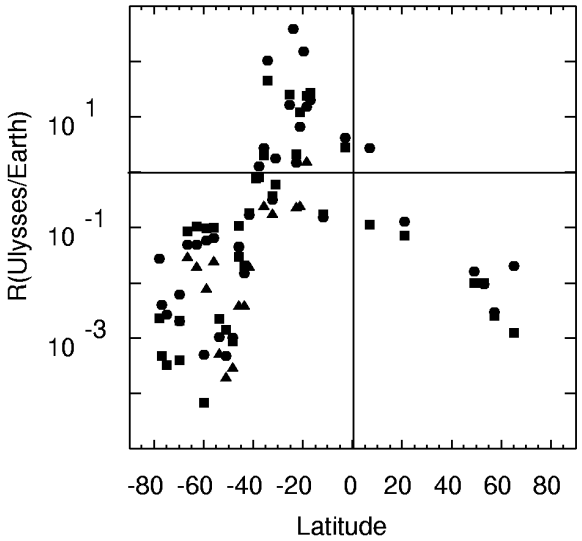

Figure 25. Latitude variation of Ulysses event intensities, normalized to the event intensity at Earth. Circles, ∼1 MeV protons; squares, ∼2 MeV protons, triangles, ∼1 MeV/amu oxygen ions.

8. High Latitude Observations

G. M. MASON

High latitude observations are covered in the accompanying chapter by Kunow, Lee *et al.* (1999). An example of the heliolatitude dependence is shown in Fig. 25, which shows the ratio of Ulysses event intensities to the intensity measured at Earth by IMP 8 and SAMPEX instruments (Richardson *et al.*, 1998). The figure covers the period from Jupiter encounter until after the north pole passage. The dependence on latitude during the inbound passage and fast latitude scan in the southern hemisphere (latitude $<0°$) may be expressed by an e-folding latitude of $6°$; however this variation also includes radial effects as Ulysses moved closer to the Sun. The northern hemisphere e-folding latitude, based on a smaller number of data points, is slightly larger ($8°$) (Richardson *et al.*, 1998). The peak ratio of Ulysses to 1 AU measurements occurs within $36°$ of the ecliptic with Ulysses at >4.5 AU, consistent with earlier observations that CIR intensities are higher at several AU than at 1 AU. For other details see the accompanying paper by Kunow, Lee *et al.* (1999).

9. Summary of Key Observational Features

G. M. MASON

A number of new observational features (Tab. IV) have been established that must be fitted by any theory of CIR energetic particle acceleration and transport. The

TABLE IV
Key Observational features of CIR energetic particles

Source location	· peak intensity at 4 AU with $1/r^2$ fall off at large distances · peak intensity at $\sim 20°$ latitude with e-folding distance 6–8°
Transport	· at 1 AU observe generally sunward flow · puzzling non field aligned flow at peak intensities at 1 AU · transport of CIR ions to latitudes well above shock locations · varying ratio of He^+ to He^{++} from 1 to ~ 5 AU implies poor inward transport of low energy He^+ at tens of keV/amu · strong inhibition of particle transport across stream interface
Spectral forms	· power law from tens of keV/amu to ~ 1 MeV/amu · steepening above ~ 1 MeV/amu · spectral forms do not change out to large (tens of AU) distances
Acceleration mechanism	· ion intensity peaks coincide with forward and reverse shocks · low energy (tens of keV) ions at 1 AU observed even in absence of shocks · same time-intensity profiles from He through Fe implies Q/M independence of acceleration mechanism · mechanism to produce electrons 50 keV to a few hundred keV at several AU; small intensities at 1 AU
Composition and seed population	· similar to solar system except for factor 2–3 enhancement of He and C relative to O · increase of He/O and Ne/O ratios with solar wind speed · He abundance increases from 1 to 5 AU · Mg/O ratio same in both forward and reverse shock periods, and close to average of slow and fast solar wind stream values · relation of composition to pick up ion sources in heliosphere: local interstellar neutrals, dust, and others?

source location of the CIR particles may be gauged by the peak of the intensities, which occurs at about 4 AU heliocentric distance, and decreases as approximately $1/r^2$ at greater distances. In terms of heliolatitude, the peak intensities are observed at about 20° latitude, with a e-folding angle of 6–8°. The *transport* of the particles to the inner solar system results in an overall sunward flow in the plasma frame. In some intense CIR events, non-field aligned flow has been observed, which coincides with the peak fluxes and continues for 12–24 hours. An additional puzzle in CIR transport is the observation of CIR ions at high heliolatitudes, far away from the shocks.

The *spectral form* of CIR ions is a power law from ∼10 keV/amu to 1 MeV/amu, with a steepening of the spectrum above 1 MeV/amu. At the higher energies, the spectral form shows little or no change out to tens of AU. The *acceleration mechanism* should produce spectral forms at the forward and reverse shocks that can be calculated from the observed compression ratios at distances of several AU, where the CIR shocks are well-formed. At 1 AU, where there are often no shocks observed, the presumed local acceleration of low energy ions (tens of keV/amu) must also be explained. The acceleration mechanism must be independent of Q/M (charge/mass) for ions over the range from He through Fe, since the time-intensity profiles for these species are the same. The mechanism must also explain the presence of electrons of energies 50 to a few hundred keV, as well as the fact that the electron intensities at several AU are much higher at the reverse shock than at the forward shock. At 1 AU, CIR electron fluxes are generally very low.

The *ion composition* and *seed population(s)* must be generally similar to solar system abundances but with some differences that need to be understood (see the accompanying paper by Scholer, Mann *et al.*, 1999). For example the abundance of pick-up He^+ near 1 AU is ∼20% of all He, while at 4.9 AU it *exceeds* the He^{++} by a large margin. The seed population implications of this fact need to be understood, as well as the implications for transport, since the larger abundances of He^+ seen at 4.9 AU do not make it into 1 AU in spite of the generally sunward flow of CIR ions. The C/O and Ne/O ratios are observed to be a strong function of solar wind speed, while other ratios such as He/O do not show this variation.

These properties are summarized in Table IV. In the next chapter, the current theoretical status for CIR energetic particle sources, acceleration, and transport is reviewed.

References

Balogh, A., Beek, T. J., Forsyth, R. J., Hedgecock, P. C., Marquedant, R. J., Smith, E. J., Southwood, D. J., and Tsurutani, B. T.: 1992, 'The Magnetic Field Investigation on the Ulysses Mission: Instrumentation and Preliminary Scientific Results', *Astron. Astrophys. Suppl.* **92**, 221–236.

Balogh, A., Gonzalez-Esparza, J. A., Forsyth, R. J., Burton, M. E., Goldstein, B. E., Smith, E. J., and Bame, S. J.: 1995, 'Interplanetary Shock Waves: Ulysses Observations in and out of the Ecliptic Plane', *Space Sci. Rev.* **72**, 171–180.

Bame, S. J., McComas, D. J., Barraclough, B. I., Phillips, J. L., Sofaly, K. J., Chaves, J. C., Goldstein, B. E., and Sakurai, R. K.: 1992, 'The Ulysses Solar Wind Plasma Experiment', *Astron. Astrophys. Suppl.* **92**, 237–265.

Bame, S. J., Goldstein, B. E., Gosling, J. T., Harvey, J. W., McComas, D. J., Neugebauer, M., and Phillips, J. L.: 1993, 'Ulysses Observations of a Recurrent High Speed Solar Wind Stream and the Heliomagnetic Streamer Belt', *Geophys. Res. Letters* **20**, 2323–2326.

Barnes, C. W., and Simpson, J. A.: 1976, 'Evidence for Interplanetary Acceleration of Nucleons in Corotating Interaction Regions', *Astrophys. J.* **210**, L91–L96.

Chotoo, K.: 1998, 'Measurements of H^+ and He^{2+} in Corotating Interaction Regions at 1 AU', *Ph.D. thesis*, Department of Physics, University of Maryland, College Park, MD, USA.

Chotoo, K., Galvin, A. B., Gloeckler, G., Hamilton, D. C., Mason, G. M., Schwadron, N. A., and Collier, M. R.: 1999, 'Composition and Spectral Measurements of H^+, He^{2+}, and He^+ in CIRs at 1 AU', *J. Geophys. Res.*, in press.

Classen, H.-T., Mann, G., and Keppler, K.: 1998, 'Particle Acceleration Efficiency and MHD Characteristics of CIR-Related Shocks', *Astron. Astrophys.* **335**, 1101–1110.

Crooker, N. U., Gosling, J. T., Bothmer, V., Forsyth, R. J., Gazis, P. R., Hewish, A., Horbury, T. S., Intriligator, D. S., Jokipii, J. R., Kóta, J., Lazarus, A. J., Lee, M. A., Lucek, E., Marsch, E., Posner, A., Richardson, I. G., Roelof, E. C., Schmidt, J. M., Siscoe, G. L., Tsurutani, B. T., and Wimmer-Schweingruber, R. F.: 1999, 'CIR Morphology, Turbulence, Discontinuities, and Energetic Particles', *Space Sci. Rev.*, this volume, 179–220.

Decker, R. B., Pesses, M. E., and Krimigis, S. M.: 1981, 'Shock-Associated Low Energy Ion Enhancements Observed by Voyagers 1 and 2', *J. Geophys. Res.* **86**, 8,819–8,831.

Decker, R. B., Krimigis, S. M., McNutt, R. L., Hamilton, D. C., and Collier, M. R.: 1995, 'Latitude-Associated Differences in the Low Energy Charged Particle Activity at Voyagers 1 and 2 during 1991 to Early 1994', *Space Sci. Rev.* **72**, 347–352.

Desai, M. I., Marsden, R. G., Sanderson, T. R., Balogh, A., Forsyth, R. J., and Gosling, J. T.: 1997, 'Particle Acceleration at Corotating Reverse Shocks in the Southern Hemisphere: Ulysses Results', *Geophys. Res. Lett.* **24**, 1155–1158.

Desai, M. I., Marsden, R. G., Sanderson, T. R., Balogh, A., Forsyth, R. J., and Gosling, J. T.: 1998, 'Particle Acceleration at Corotating Interaction Regions in the Three-Dimensional Heliosphere', *J. Geophys. Res.* **103**, 2,003–2,014.

Desai, M. I., Marsden, R. G., Sanderson, T. R., Lario, D., Roelof, E. C., Simnett, G. M., Gosling, J. T., Balogh, A., and Forsyth, R. J.: 1999, 'Energy Spectra of 50-keV to 20-MeV Protons Accelerated at Corotating Interaction Regions at Ulysses', *J. Geophys. Res.* **104**, 6,705–6,719.

Dwyer, J. R., Mason, G. M., Mazur, J. E., Jokipii, J. R., von Rosenvinge, T. T., and Lepping, R. P.: 1999, 'Perpendicular Transport of Low Energy Corotating Interaction Region-Associated Nuclei', *Astrophys. J.* **490**, L115–L118.

Edmiston, J. P., and Kennel, C. F.: 1984, 'A Parametric Survey of First Critical Mach Number for a Fast MHD shock', *J. Plasma Phys.* **32**, 411.

Fisk, L. A.: 1996, 'Motion of the Footpoints of Heliospheric Magnetic Field Lines at the Sun: Implications for Recurrent Energetic Particle Events at High Heliographic Latitudes', *J. Geophys. Res.* **101**, 15,547–15,553.

Fisk, L. A., and Lee, M. A.: 1980, 'Shock Acceleration of Energetic Particles in Corotating Interaction Regions in the Solar Wind', *Astrophys. J.* **237**, 620–626.

Fisk, L. A., and Jokipii, J. R.: 1999, 'Mechanisms for Latitudinal Transport of Energetic Particles in the Heliosphere', *Space Sci. Rev.*, this volume, 115–124.

Fränz, M., Keppler, E., Lauth, U., Reuss, M. K., Mason, G. M., and Mazur, J. E.: 1999, 'Energetic Particle Abundances at CIR Shocks', *Geophys. Res. Lett.* **25**, 17–20.

Gazis, P., McDonald, F. B., Burger, R. A., Chalov, S., Decker, R. B., Dwyer, J., Intriligator, D. S., Jokipii, J. R., Lazarus, A. J., Mason, G. M., Pizzo, V. J., Potgieter, M. S., Richardson, I. G., and

Lanzerotti, L. J.: 1999, 'Corotating Interaction Regions in the Outer Heliosphere', *Space Sci. Rev.*, this volume, 269–305.
Geiss, J., and Witte, M.: 1996, 'Properties of the Interstellar Gas Inside the Heliosphere', *Space Sci. Rev.* **78**, 229–238.
Gloeckler, G.: 1999, 'Observation of Injection and Pre-Acceleration Processes in the Slow Solar Wind', *Space Sci. Rev.*, this volume, 91–104.
Gloeckler, G., and Geiss, J.: 1998, 'Interstellar and Inner Source Pickup Ions Observed with SWICS on Ulysses', *Space Sci. Rev.* **86**, 127–159.
Gloeckler, G. *et al.*: 1992, 'The Solar Wind Ion Composition Spectrometer', *Astron. Astrophys. Suppl.* **92**, 267–289.
Gloeckler, G., Geiss, J., Roelof, E. C., Fisk, L. A., Ipavich, F. M., Ogilvie, K. W., Lanzerotti, L. J., von Steiger, R., and Wilken, B.: 1994, 'Acceleration of Interstellar Pickup Ions in the Disturbed Solar Wind Observed on Ulysses', *J. Geophys. Res.* **99**, 17,637–17,643.
Gloeckler, G. *et al.*: 1995, 'The Solar Wind and Suprathermal Ion Composition Investigation on the WIND Spacecraft', *Space Sci. Rev.* **71**, 79–124.
Gloeckler, G., Fisk, L. A., and Geiss, J.: 1997, 'Anomalously Small Magnetic Field in the Local Interstellar Cloud', *Nature* **386**, 374–377.
Gold, R. E., Lanzerotti, L. J., Maclennan, C. G., and Krimigis, S. M.: 1986, 'Latitude Dependence of Corotating Shock Acceleration in the Outer Heliosphere', *in* R. G. Marsden and D. Reidel (eds.), *The Sun and the Heliosphere in Three Dimensions*, Hingham, Mass. p. 325.
Gold, R. E., Decker, R. B., Lanzerotti, L. J., and Maclennan, C. G.: 1988, 'The Latitude and Radial Dependence of Shock Acceleration in the Heliosphere', *J. Geophys. Res.* **93**, 991–996.
Gold, R. E., Decker, R. B., Krimigis, S. M., and Lanzerotti, L. J.: 1991, 'The Extent and Symmetry of Shocks in the Outer Heliosphere', *Proc. 22nd Internat. Cosmic Ray Conf.* **3**, 605–608.
Gosling, J. T., and Robson, A. E..: 1985, 'Ion Reflection, Gyration, and Dissipation at Supercritical Shocks', *in* R. G. Stone and B. T. Tsurutani (eds.), *Collisionless Shocks in the Heliosphere: A Tutorial Review*, AGU Monograph 35, Washington DC, pp. 141–151.
Gosling, J. T., Thomsen, M. F., Bame, S. J., Feldman, W. C., Paschmann, G., and Sckopke, N.: 1982, 'Evidence for Specularly Reflected Ions Upstream from Quasi-parallel Bow Shock', *Geophys. Res. Lett.* **9**, 1333–1337.
Gosling, J. T., Bame, S. J., Feldman, W. C., McComas, D. J., Phillips, J. L., and Goldstein, B. E.: 1993a, 'Counterstreaming Suprathermal Electron Events Upstream of Corotating Shocks in the Solar Wind beyond $\sim$2 AU: Ulysses', *Geophys. Res. Lett.* **20**, 2335–2338.
Gosling, J. T., Bame, S. J., McComas, D. L., Phillips, J. L., Pizzo, V. J., Goldstein, B. E., and Neugebauer, M.: 1993b, 'Latitudinal Variation of Solar Wind Corotating Stream Interaction Regions: Ulysses', *Geophys. Res. Lett.* **20**, 2789–2792.
Hamilton, D. C., Gloeckler, G., Armstrong, T. P., Axford, W. I., Bostrom, C. O., Fan, C. Y., Krimigis, S. M., and Lanzerotti, L. J.: 1978, 'Composition of Corotating Particle Events Observed by Voyager 2 in 1978', *Proc. 16th Internat. Cosmic Ray Conf.* **5**, 363–367.
Hilchenbach, M., Grünwaldt, H., Kucharek, H., Klecker, B., Hovestadt, D., Kallenbach, R., Bochsler, P., Gliem, F., Galvin, A. B., Chotoo, K., and Ipavich, F. M.: 1997, 'Charge State Composition of Energetic Helium as Observed in CIRs at 1 AU with SOHO/CELIAS', *Trans. Am. Geophys. U.* **78**, F554.
Hovestadt, D., Klecker, B., Gloeckler, G., Ipavich, F. M., and Scholer, M.: 1984, 'Survey of He^{+}/He^{++} Abundance Ratios in Energetic Particle Events', *Astrophys. J. Lett.* **282**, L39–L42.
Hovestadt, D. *et al.*: 1995, 'CELIAS: The Charge, Element, and Isotope Analysis System for SOHO', *Sol. Phys.* **162**, 441–481.
Hundhausen, A. J., and Gosling, J. T.: 1976, 'Solar Wind Structure at Large Heliospheric Distances: An Interpretation of Pioneer 10 Observations', *J. Geophys. Res.* **81**, 1,436–1,440.

Kane, M., Decker, R. B., Mauk, B. H., and Krimigis, S. M.: 1995, 'Latitudinal and Radial Variation of Shock Associated $\geq$30 keV Ion Spectra and Anisotropies at Voyagers 1 and 2', *Space Sci. Rev.* **72**, 353–358.

Kennel, C. F., Edmiston, J. P., and Hada, T.: 1985, 'A Quarter Century of Collisionless Shock Research', *in* R. G. Stone and B. T. Tsurutani (eds.), *Collisionless Shocks in the Heliosphere: A Tutorial Review*, AGU Monographs 34, Washington DC, pp. 1–36.

Keppler, E., Blake, J. B., Hovestadt, D., Korth, A., Quenby, J., Umlauft, G., and Woch, J.: 1992, 'The Ulysses Energetic Particle Composition Experiment EPAC', *Astron. Astrophys. Suppl.* **92**, 317–331.

Kóta, J., and Jokipii, J. R.: 1983, 'Effects of Drift on the Transport of Cosmic Rays', *Astrophys. J.* **265**, 573–581.

Krimigis, S. M., Armstrong, T. P., Axford, W. I., Bostrom, C. O., Fan, C. Y., Gloeckler, G., and Lanzerotti, L. J.: 1977, 'The Low Energy Charged Particle (LECP) Instrument on the Voyager Spacecraft', *Space Sci. Rev.* **21**, 329–354.

Krimigis, S. M., Decker, R. B., Hamilton, D. C., and Hill, M. E.: 1997, 'Energetic Ions in the Outer Heliosphere', 1992-1997, *Proc. 25th Internat. Cosmic Ray Conf.* **1**, 393–396.

Kunow, H., Lee, M. A., Fisk, L. A., Forsyth, R. J., Heber, B., Horbury, T. S., Keppler, E., Kóta, J., Lou, Y.-Q., McKibben, R. B., Paizis, C., Potgieter, M. S., Roelof, E. C., Sanderson, T. R., Simnett, G. M., von Steiger, R., Tsurutani, B. T., Wimmer-Schweingruber, R. F., and Jokipii, J. R.: 1999, 'Corotating Interaction Regions at High Latitudes', *Space Sci. Rev.*, this volume, 221–268.

Lanzerotti, L. J., Venkatesan, D., and Wibberenz, G.: 1973, 'Rise Time to Maximum Flux of Relativistic Solar Electron Events and its Relation to the High-Frequency Component of the Interplanetary Field Power Spectrum', *J. Geophys. Res.* **78**, 7,986–7,995.

Lanzerotti, L. J., Gold, R. E., Anderson, K. A., Armstrong, T. P., Lin, R. P., Krimigis, S. M., Pick, M., Roelof, E. C., Sarris, E. T., Simnett, G. M., and Frain, M. E.: 1992, 'Heliospheric Instrument for Spectra, Composition, and Anisotropies at Low Energies', *Astron. Astrophys. Suppl.* **92**, 349–363.

Lazarus, A., Richardson, J. D., Decker, R. B., and McDonald, F. B.: 1999, 'Voyager 2 Observation of Corotating Interaction Regions (CIRs) in the Outer Heliosphere', *Space Sci. Rev.*, this volume, 53–59.

Lepping, R. P. *et al.*: 1995, 'The Wind Magnetic Field Investigation', *Space Sci. Rev.* **71**, 207–229.

Marsden, R. G., Smith, E. J., Cooper, J. F., and Tranquille, C.: 1996, 'Ulysses at High Heliographic Latitudes: An Introduction', *Astron. Astrophys.* **316**, 279–286.

Marshall, W.: 1955, 'The Structure of Magnetohydrodynamic Shock Waves', *Proc. R. Soc. London, Ser. A* **233**, 367–372.

Mason, G. M., Mazur, J. E., Dwyer, J. R., Reames, D. V., and von Rosenvinge, T. T.: 1997, 'New Spectral and Abundance Features of Interplanetary Heavy Ions in Corotating Interaction Regions', *Astrophys. J.* **486**, L149–L152.

Mason, G. M., and Sanderson, T. R.: 1999, 'CIR Associated Energetic Particles in the Inner and Middle Heliosphere', *Space Sci. Rev.*, this volume, 77–90.

Ogilvie, K. W. *et al.*: 1995, SWE, 'A Comprehensive Plasma Instrument for the Wind Spacecraft', *Space Sci. Rev.* **71**, 55–77.

Palmer, I. D., and Gosling, J. T.: 1978, 'Shock-Associated Energetic Proton Events at Large Heliocentric Distances', *J. Geophys. Res.* **83**, 2,037–2,046.

Priest, E. R.: 1982, 'Solar Magneto-Hydromagnetics', *in* D. Reidel (ed.), Geophysics and Astrophysics Monographs 21, Dordrecht.

Richardson, I. G., Mazur, J. E., and Mason, G. M.: 1998, 'A Comparison of Recurrent Energetic Ion Enhancements Observed at Ulysses and at 1 AU by IMP 8 and SAMPEX: Ulysses Launch until Following the First North Polar Passage', *J. Geophys. Res.* **103**, 2,115–2,129.

Riley, P., Gosling, J. T., Weiss, L. A., and Pizzo, V. J.: 1996, 'The Tilts of Corotating Interaction Regions at Midheliographic Latitudes', *J. Geophys. Res.* **101**, 24,349–24,357.

Sanderson, T. R., Marsden, R. G., Wenzel, K.-P., Balogh, A., Forsyth, R. J., and Goldstein, B. E.: 1994, 'Ulysses High-Latitude Observations of Ions Accelerated by Corotating Interaction Regions', *Geophys. Res. Lett.* **21**, 1113–1116.

Scholer, M., Mann, G., Chalov, S., Desai, M. I., Fisk, L. A., Jokipii, J. R., Kallenbach, R., Keppler, E., Kóta, J., Kunow, H., Lee, M. A., Sanderson, T. R., and Simnett, G. M.: 1999, 'Origin, Injection, and Acceleration of CIR Particles', *Space Sci. Rev.*, this volume, 369–399.

Schwadron, N. A., Fisk, L. A., and Gloeckler, G.: 1996, 'Statistical Acceleration of Interstellar Pick-up Ions in Corotating Interaction Regions', *Geophys. Res. Lett.* **23**, 2871–2874.

Schwartz, S. J., Thomsen, M. F., and Gosling, J. T.: 1983, 'Ions Upstream of the Earth's Bow Shock: A Theoretical Comparison of Alternative Source Population', *J. Geophys. Res.* **88**, 2,039–2,045.

Sckopke, N., Paschmann, G., Bame, S. J., Gosling, J. T., and Russell, C. T.: 1983, 'Evolution of Ion Distributions Across the Nearly Perpendicular Bow Shock: Specularly and Nonspecularly Reflected Gyrating Ions', *J. Geophys. Res.* **88**, 6,121–6,131.

Simnett, G. M., Sayle, K. A., Roelof, E. C., and Tappin, S. J.: 1994, 'Corotating Particle Enhancements out of the Ecliptic Plane', *Geophys. Res. Letters* **21**, 1561–1564.

Simnett, G. M. and Roelof, E. C.: 1997, 'Acceleration and Modulation of Energetic Particles in the 3-D heliosphere by Corotating Interaction Regions', *Adv. Space Res.* **19**, 859–868.

Simpson, J. A., Anglin, J. D., Balogh, A., Bercovitch, M., Bouman, J. M., Budzinski, E. E., Burrows, J. R., Carvell, R., Connell, J. J., and Ducros, R.: 1992, 'The Ulysses Cosmic Ray and Solar Particle Investigation', *Astron. Astrophys. Suppl.* **92**, 365–399.

Thomsen, M. F., Gosling, J. T., Bame, S. J., and Russell, C. T.: 1985, 'Gyrating Ions and Large-Amplitude, Monochromatic MHD Waves of Earth's Bow Shock', *J. Geophys. Res.* **90**, 267–275.

Tsurutani, B. T., Smith, E. J., Pyle, K. R., and Simpson, J. A.: 1982, 'Energetic Protons Accelerated at Corotating Shocks: Pioneer 10 and 11 Observations from 1 to 6 AU', *J. Geophys. Res.* **87**, 7,389–7,404.

von Rosenvinge, T. T. *et al.*: 1995, 'The Energetic Particles Acceleration, Composition, and Transport (EPACT) Investigation on the WIND Spacecraft', *Space. Sci. Rev.* **71**, 155–206.

von Steiger, R., Geiss, J., and Gloeckler, G.: 1997, 'Composition of the Solar Wind', *in* J. R. Jokipii, C. P. Sonnett, and M. S. Giampapa (eds.), *Cosmic Winds and the Heliosphere*, Univ. of Arizona Press, Tucson, pp. 581–616.

Wimmer–Schweingruber, R. F., von Steiger, R., and Paerli, R.: 1997, 'Solar Wind Stream Interfaces in Corotating Interaction Regions: SWICS/Ulysses Results', *J. Geophys. Res.* **102**, 17,407–17,417.

Address for Offprints: G. M. Mason, Department of Physics, University of Maryland, College Park, Maryland 20742, USA (Glenn.Mason@umail.umd.edu)